Engineered Science
DOI: https://dx.doi.org/10.30919/es1586

Research on the Nonlinear Structural Dynamic Characteristics of the Rigid Flexible Coupling Folding Wing Model for Aircraft

Xinqiang Lu, Rui Yang and Shiyong Sun*

Abstract

During the working process of the folding wing, there is not only a large-range rigid body motion but also a deformation motion of the flexible components. The problem of the rigid-flexible coupling of the structure is extremely complex. Aiming at this problem, this study proposes a nonlinear dynamic model of the rigid-flexible coupling structure of the folding wing, revealing the coupling effect between the large-range rotational motion and the flexible deformation. The research results show that the dynamic behavior of the system exhibits significant nonlinear characteristics. In the examples of the structural inherent properties and the transverse excitation response, the rigid-flexible coupling nonlinear numerical model has higher solution accuracy compared with the linear numerical model. Furthermore, the influence of the change of the folding angle on the inherent properties and dynamic response of the structure has been explored. Finally, an experimental model of the folding wing is designed and manufactured based on the similarity principle, which further verifies the accuracy of the rigid-flexible coupling dynamic model in solving the dynamic characteristics of the structure. The establishment of the rigid-flexible coupling model of the folding wing provides a theoretical basis for the dynamic characteristic of the folding wing structure.

Keywords: Folding wing; Structural dynamics; Aerospace engineering; Experimental research; Modelling.
Received: 18 April 2025; Revised: 29 May 2025; Accepted: 10 June 2025.
Article type: Research article.

1. Introduction

Variable geometry aircraft can significantly improve their comprehensive performance by changing their external geometric shapes, adjusting factors such as the aspect ratio and the lift-drag ratio according to local conditions. This enables the aircraft to reach an optimal compromise state in various environments.[1-3] The development of compliant variable geometry aircraft has brought many remarkable advantages, such as improving flight efficiency, increasing payload, reducing noise, saving fuel, enhancing flight flexibility, and improving the entire flight envelope.[4,5] The deformation of variable geometry aircraft is mainly reflected in the change of the geometric shape of the wings. The folding wing technology is an efficient deformation technology, and the flexible variable geometry folding wing technology is widely applied in variable geometry aircraft.

In recent years, great progress has been made in the structural design of folding wings. In terms of the mechanical structure, it has evolved from the initial single degree of freedom rotation connected by a rigid hinge to multi-degree of freedom compliant rotation in various flexible ways.[6,7] The folding wing structure has gradually formed a rigid-flexible coupling structure integrating intelligent materials, flexible honeycomb structures, compliant corrugated plate structures, *etc*.[8,9] Lv designed a dual-joint folding wing deployment mechanism and studied the rigid-flexible coupling dynamics modeling and related technologies of the folding wing based on this structure.[10] Chang proposed an aerodynamic optimization design method for double folding wings considering the geometric constraints of the second deployment mechanism under the condition of considering multiple geometric constraints.[11] Zhao designed and developed a structural model that realizes the rapid deployment of the longitudinally folding wing through the composite drive of burnt gunpowder and a compression spring.[12]

The theories of the structural dynamics characteristics and aeroelastic dynamics characteristics of folding wings have been deeply studied. Li and Chen studied the nonlinear

School of Mechanical Engineering, Dalian University of Technology, Dalian, 116024, China
**Email:* sunshy@dlut.edu.cn (S. Sun)

aeroelastic characteristics of variable geometry wings when the wing Folding angle is between 0° and 30°.[13] Huang explored the dynamic aerodynamic characteristics of Z-shaped folding wings at different folding speeds.[14] Hu used the flexible multi-body dynamics method to model the folding process of the variable geometry wing structure and calculate the aerodynamic force of the wing.[15] Fu focused on studying the vibration suppression and attitude control problems of flapping wing unmanned aerial vehicles with rigid-flexible coupling wings.[16] Huang and Zhou proposed a new parametric modeling method for efficient modal and nonlinear aeroelastic analysis of folding wings with bilinear hinge stiffness and changing Folding angles.[17] Yang proposed an analysis method of the substructure modal synthesis method with optimized boundary conditions, which can analyze the dynamic characteristics of the structure more quickly.[18]

Most of the above-mentioned studies focus on the aerodynamic characteristics of folding wings and the analysis under the static wing configuration, and some studies have investigated the flexible deformation and geometric nonlinear dynamics characteristics of the wings in real situations.[19] Huang proposed an equivalent modeling method for a two-dimensional flexible wing with an out of dihedral angle deformation based on a non-uniform beam model.[20] Xu derived the dynamic equations of geometrically nonlinear beam structures based on Hamilton's principle considering the flexible characteristics of the wings.[21] Guo studied the structural nonlinear dynamics characteristics of folding wings in subsonic fluids based on the thin wing theory under the condition of an ideal incompressible fluid.[22] Marcstated established an aeroelastic model of the variable geometry wing structure using the unsteady vortex lattice method and proposed a method to calculate its nonlinear aeroelastic characteristics during flight.[23] Tian proposed a novel approximate global mode method (AGMM) for dealing with complex boundary conditions and models a folding wing consisting of separate rectangular plates for nonlinear flutter analysis.[24] Qi used a quasi-steady-state computational algorithm to obtain the steady-state aerodynamic characteristics of a Z-folded wing at various angles of attack and flow velocities, and developed a dynamic mesh method capable of instantaneous reconstruction.[25] Yan and Pu all designed the folding wing structure from the bionic design point of view and analysed its dynamic characteristics.[26,27]

As indicated by the preceding discussion, past theoretical studies have greatly contributed to our understanding of the aerodynamic and vibrational characteristics of folding wings. However, most research on variant wings is mainly based on the idea of fixed wings, which breaks down the variant process into centralized fixed state modeling and analysis, lacking a structural dynamics modeling method applicable to variant structures; In addition, during the operation of folding wings, there is a large range of rigid body motion and deformation motion of flexible components. There is relatively little research on the vibration characteristics of the rigid flexible coupling structure of folding wings, and there is also a lack of research dedicated to its verification and analysis. Aiming at these problems, the current study conducts research on the nonlinear dynamics characteristics of the rigid-flexible coupling structure of folding wings. It simplifies the structure into a thin plate system composed of a rigid inner wing and a flexible outer wing. By establishing an inertial and a floating coordinate system, based on the hybrid coordinate method, Kirchhoff's thin plate theory, the assumed mode method, and Lagrange's equations, the rigid-flexible coupling nonlinear dynamics equations are constructed to reveal the strong coupling effect between large-range rotation and flexible deformation. By changing parameters such as the driving torque and transverse excitation, the influence of the rigid-flexible coupling phenomenon on the structural dynamics characteristics is explored, as well as the influence of the rigid-flexible coupling nonlinear coefficient on the natural frequency of the structure. Finally, an experimental model of the folding wing is designed and manufactured based on the similarity principle, and the experimental results are used to verify the reliability of the theoretical research.

2. Modeling of the dynamic model of the rigid-flexible coupling structure

2.1 Theoretical model of the folding wing

Based on the structure of the folding wing, the wing is simplified into a two-plate rigid-flexible coupling system composed of a rigid thin plate and a flexible thin plate. The inner wing structure is simplified as a rigid structural plate, with a length of a_1, a width of b_1. One end of the rigid plate rotates at a low speed around the Y-axis, with a torque of τ_1, and a rotation angle of θ_1. The outer wing structure is simplified as a flexible plate structure, with a length of a_2, a width of b_2, a thickness of h_2, and a density of ρ_2. The structure is hinged to the inner wing, with a torque of τ_2 and a rotation angle of θ_2. According to the hybrid coordinate method, a floating coordinate system is established for the two-plate rigid-flexible coupling system. An inertial coordinate system $OXYZ$ is established for the rigid plate structure, and a floating coordinate system $oxyz$ is established for the flexible plate structure. The motion of any point P on the flexible body can be decomposed into the superposition of the large-range motion related to the floating coordinate sys-

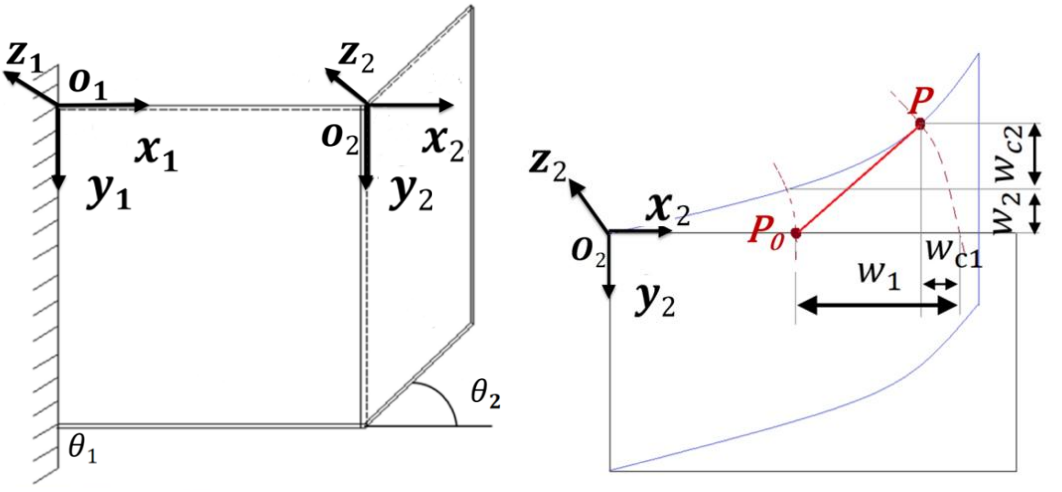

Fig. 1: Schematic diagram of the rigid-flexible coupling folding wing structure.

tem and the flexible deformation motion relative to the floating coordinate system. The schematic diagram of the folding wing structure is shown in Fig. 1.

The kinetic energy of the rigid plate structure is solved based on the inertial coordinate system $OXYZ$, as shown in Eqs. (1)-(4):

$$T_1 = \frac{1}{2} I_1 \dot{\theta}_1^2 + \frac{1}{2} M_1 \left(\frac{a_1}{2}\dot{\theta}_1\right)^2 = \frac{7}{24} {a_1}^3 b_1 h_1 \rho_1 \dot{\theta}_1^2 \quad (1)$$

$$M_1 = \iiint_{V_1} \rho_1 \, dV_1 \quad (2)$$

$$I_1 = \frac{1}{3} M_1 {a_1}^2 \quad (3)$$

$$U_1 = \frac{1}{2} M_1 g a_1 sin\theta_1 = \frac{1}{2} {a_1}^2 b_1 h_1 \rho_1 g sin\theta_1 \quad (4)$$

where T_1 represents the kinetic energy of the rigid plate, U_1 represents the potential energy of the rigid plate, b represents the length of the rigid plate, a represents the width of the rigid plate, h_1 represents the thickness of the rigid plate, ρ_1 represents the density of the rigid plate, I_1 represents the moment of inertia of the rigid plate, and M_1 represents the mass of the rigid plate.

2.2 Structural dynamics modelling

The motion of any arbitrary point P on the flexible body can be decomposed into the deformation of the floating coordinate system. The displacements along the x, y, and z directions are $u_1(x,y,z,t)$, $u_2(x,y,z,t)$ and $u_3(x,y,z,t)$ in Eqs. (5)-(10):

$$u_1(x,y,z,t) = w_1(x,y,t) - w_{c1}(x,y,t) = w_1 - \frac{1}{2}\int_0^x \left(\frac{\partial u_3}{\partial x}\right)^2 dx \quad (5)$$

$$u_2(x,y,z,t) = w_2(x,y,t) - w_{c2}(x,y,t) = w_2 - \frac{1}{2}\int_0^y \left(\frac{\partial u_3}{\partial y}\right)^2 dy \quad (6)$$

$$u_3(x,y,z,t) = w_3(x,y,t) + w_{c3}(x,y,t) = w_3 + \int_0^x \frac{\partial u_1}{\partial x}\frac{\partial u_3}{\partial x} dx + \int_0^y \frac{\partial u_2}{\partial y}\frac{\partial u_3}{\partial y} dy \quad (7)$$

$$()w_{c1}(x,y,t) = \frac{1}{2}\int_0^x \left(\frac{\partial u_3}{\partial x}\right)^2 dx \quad (8)$$

$$w_{c2}(x,y,t) = \frac{1}{2}\int_0^y \left(\frac{\partial u_3}{\partial y}\right)^2 dy \quad (9)$$

$$w_{c3}(x,y,t) = u_3 + \int_0^x \frac{\partial u_1}{\partial x}\frac{\partial u_3}{\partial x} dx + \int_0^y \frac{\partial u_2}{\partial y}\frac{\partial u_3}{\partial y} dy \quad (10)$$

where $u_1(x,y,z,t)$, $u_2(x,y,z,t)$, and $u_3(x,y,z,t)$ are the displacements of any point on the plate in the x, y, and z directions in the Cartesian coordinate system. $w_1(x,y,t)$ and $w_2(x,y,t)$ are the deformation elongation amounts of point P_0 along the z-direction in the x and y directions. $w_{c1}(x,y,t)$、$w_{c2}(x,y,t)$ and $w_{c3}(x,y,t)$ are the coupling nonlinear deformation amounts. The coupling nonlinear deformation amounts $w_{c1}(x,y,t)$ and $w_{c2}(x,y,t)$ are caused by the compression deformation of the thin plate in the x and y directions due to the deformation in the z-direction; the coupling nonlinear deformation amount w_{c3} is caused by the stretching deformation of the thin plate in the z-direction due to the deformation in the x and y directions. The deformation amount in the z direction is much larger than that in the x and y directions, therefor, $w_{c3}(x,y,t) \approx 0$ .When the coupling nonlinear deformation amount is taken into account, the correction model is a rigid-flexible coupling model. Otherwise, it is a linear model.

The deformation displacement $u_{i0}(u_{10}, u_{20}, u_{30})$ of any point P^* on the non-neutral surface of the thin plate relative to the floating base can be related to the deformation

displacement of the corresponding point on the neutral surface, as presented in Eqs. (11)-(13):

$$u_{10}(x,y,z,t) = u_1 - z\frac{\partial u_3}{\partial x} = w_1 - \frac{1}{2}\int_0^x \left(\frac{\partial u_3}{\partial x}\right)^2 dx - z\frac{\partial u_3}{\partial x} \quad (11)$$

$$u_{20}(x,y,z,t) = u_2 - z\frac{\partial u_3}{\partial y} = w_1 - \frac{1}{2}\int_0^y \left(\frac{\partial u_3}{\partial y}\right)^2 dy - z\frac{\partial u_3}{\partial y} \quad (12)$$

$$u_{30}(x,y,z,t) = u_3 = w_3 \quad (13)$$

Since the theoretical model of the folded wing belongs to a thin plate structure and the planar radial dimensions of the structure are much larger than the thickness dimensions, the Kirchhoff theory, which responds to the mechanical properties of the thin plate, can be used, and Li *et al*.[28] also used this theory in analysing the dynamic properties of the plate structure. The modelling is based on the Kirchhoff theory, it is assumed that the normal line perpendicular to the mid-surface before the structural deformation remains perpendicular to the current mid-surface during the deformation process. Therefore, the shear strains γ_{zy} and γ_{zx} generated in the z-direction of the structure can be ignored. In addition, as it is a thin-plate structure, the thickness of the plate is much smaller than its length and width, so the strain ε_{zz} in the z-direction can be ignored. The relationship between the geometric nonlinear displacement and strain at any point of the flexible plate structure is as shown in the following Eqs. (14)-(16):

$$\varepsilon_{xx} = \frac{\partial u_{10}}{\partial x} + \frac{1}{2}\left(\frac{\partial u_{30}}{\partial x}\right)^2 = \frac{\partial w_1}{\partial x} - z\frac{\partial^2 w_3}{\partial^2 x} \quad (14)$$

$$\varepsilon_{yy} = \frac{\partial u_{20}}{\partial y} + \frac{1}{2}\left(\frac{\partial u_{30}}{\partial y}\right)^2 = \frac{\partial w_2}{\partial y} - z\frac{\partial^2 w_3}{\partial^2 y} \quad (15)$$

$$\gamma_{xy} = \frac{\partial u_{20}}{\partial x} + \frac{\partial u_{10}}{\partial y} + \frac{\partial u_{30}}{\partial x}\frac{\partial u_{30}}{\partial y} = \frac{\partial w_2}{\partial x} + \frac{\partial w_1}{\partial y} - 2z\frac{\partial w_3}{\partial x}\frac{\partial w_3}{\partial y} \quad (16)$$

According to the physical equations of elastic mechanics, the relationship between the stress and strain of the plate is as follows using Eqs. (17)-(20).

$$\sigma_{xx} = -\frac{E}{1-\mu^2}\left(\varepsilon_{xx} + \mu\varepsilon_{yy}\right) = -\frac{E}{1-\mu^2}\left(\frac{\partial w_1}{\partial x} - z\frac{\partial^2 w_3}{\partial^2 x} + \mu\frac{\partial w_2}{\partial y} - z\mu\frac{\partial^2 w_3}{\partial^2 y}\right) \quad (17)$$

$$\sigma_{yy} == -\frac{E}{1-\mu^2}\left(\varepsilon_{yy} + \mu\varepsilon_{xx}\right) = -\frac{E}{1-\mu^2}\left(\frac{\partial w_2}{\partial y} - z\frac{\partial^2 w_3}{\partial^2 y} + \mu\frac{\partial w_1}{\partial x} - z\mu\frac{\partial^2 w_3}{\partial^2 x}\right) \quad (18)$$

$$\tau_{xy} = G * \left(\frac{\partial w_2}{\partial x} + \frac{\partial w_1}{\partial y} - 2z\frac{\partial u_{30}}{\partial x}\frac{\partial u_{30}}{\partial y}\right) \quad (19)$$

$$G = \frac{E}{2(1+\mu)} \quad (20)$$

where σ_{xx} is the normal stress in the x-direction, σ_{yy} is the normal stress in the y-direction, τ_{xy} is the shear stress, E is the elastic modulus of the flexible plate, μ is Poisson's ratio, and G is the shear modulus.

The deformation displacements $w_1(x,y,t)$, $w_2(x,y,t)$ and $w_3(x,y,t)$ of the flexible plate structure in the $x, y,$ and z directions are discretized by the assumed-mode method. The discretization of displacement deformation is as shown in Eqs. (21)-(23).

$$w_1(x,y,t) = \emptyset_1(x,y)q_1(t) \quad (21)$$

$$w_2(x,y,t) = \emptyset_2(x,y)q_2(t) \quad (22)$$

$$w_3(x,y,t) = \emptyset_3(x,y)q_3(t) \quad (23)$$

where $\emptyset_1(x,y) \in R^{1\times N}$, $\emptyset_2(x,y) \in R^{1\times N}$ and $\emptyset_3(x,y) \in R^{1\times N}$ are the mode shape functions of the $1 \times N$ dimensional flexible plate structure. $q_1(t)$、$q_2(t)$ and $q_3(t)$ are the vibration mode coordinates of the $1 \times N$ dimensional flexible thin-plate structure. The vibration modes and mode coordinates of the flexible body structure correspond to each other in dimension, and N is the truncation order of the mode functions. For the convenience of expression, the independent variables $x, y,$ and t in the equation are omitted in the following text.

Substitute Eqs. (11)-(13) into Eqs. (5)-(7), and we get:

$$u_1 = w_1 - w_{c1} = \emptyset_1 q_1 - \frac{1}{2}H_1(x,y){q_3}^2 \quad (24)$$

$$u_2 = w_2 - w_{c2} = \emptyset_2 q_2 - \frac{1}{2}H_2(x,y){q_3}^2 \quad (25)$$

$$u_3 = w_3 = \emptyset_3 q_3 \quad (26)$$

$$H_1(x,y) = \int_0^x \phi_{3,x}^T \phi_{3,x} dx;\ \ H_2(x,y) = \int_0^y \phi_{3,y}^T \phi_{3,y} dy \quad (27)$$

where $H_1(x,y)$ and $H_2(x,y)$ are the mode shape functions of the coupling nonlinear deformation. The subscript ',' indicates the partial derivative with respect to the coordinate. For example, $\phi_{3,x}$ is the partial derivative of $\emptyset_3$ with respect to x.

The coordinate expression of an arbitrary point P on the flexible plate in the global coordinate system is as follows.

$$r_p = Trans + Rot \cdot [u_1\ \ u_2\ \ u_3]^T \quad (28)$$

$$Trans = [a_1 cos\theta_1\ \ 0\ \ a_1 sin\theta_1]^T \quad (29)$$

$$Rot(y,\theta_{y_2}) = \begin{bmatrix} \cos\theta_2 & 0 & -\sin\theta_2 \\ 0 & 1 & 0 \\ \sin\theta_2 & 0 & \cos\theta_2 \end{bmatrix} \quad (30)$$

where r_p is the coordinate of an arbitrary point P in the global coordinate system, Trans is the translation matrix,

and $Rot(y,\theta_2)$ is the transformation matrix for rotation about the y-axis by θ_2.

Substitute Eqs. (24)-(30) into Eq. (28), we get Eq. (31):

$$r_p = \begin{bmatrix} a_1 cos\theta_1 + cos\,\theta_2\left(x + \emptyset_1 q_1 + H_1 {q_3}^2\right) - sin\,\theta_2 \emptyset_3 q_3 \\ y + \emptyset_2 q_2 + H_2 {q_3}^2 \\ a_1 sin\theta_1 + sin\,\theta_2\left(x + \emptyset_1 q_1 + H_1 {q_3}^2\right) + cos\,\theta_2\,\emptyset_3 q_3 \end{bmatrix} \quad (31)$$

By taking the derivative of the position coordinate r_p of an arbitrary point P, the velocity of this point can be obtained, as Eq. (32) shows:

$$\dot{r_p} = \begin{bmatrix} -a_1 sin\theta_1\dot{\theta}_1 - sin\theta_2\dot{\theta}_2(x + \emptyset_1 q_1 + H_1 {q_3}^2) \\ +cos\theta_2(\emptyset_1\dot{q_1} + H_1 q_3\dot{q_3}) - cos\theta_2\dot{\theta}_2\emptyset_3 q_3 - \sin\theta_2\,\emptyset_3\dot{q_3} \\ \emptyset_2\dot{q_2} + 2H_2 q_3\dot{q_3} \\ a_1 cos\theta_1\dot{\theta}_1 + \cos\theta_2\,\dot{\theta}_2\left(x + \emptyset_1 q_1 + H_1 {q_3}^2\right) \\ + \sin\theta_2\,(\emptyset_1\dot{q_1} + H_1 q_3\dot{q_3}) - \sin\theta_2\,\dot{\theta}_2\emptyset_3 q_3 + cos\theta_2\emptyset_3\dot{q_3} \end{bmatrix} \quad (32)$$

The kinetic energy T_2 of the flexible plate structure is solved as shown in the following Eq. (33):

$$T_2 = \frac{1}{2}M_i v_i^2 = \frac{1}{2}\iiint_{V_2}\rho_2\,\dot{r_p}^T\dot{r_p}dV = \frac{1}{2}\int_0^{a_2}\int_0^{b_2}\int_{-\frac{h_2}{2}}^{\frac{h_2}{2}}\rho_2\,\dot{r_p}^T\dot{r_p}\,dxdydz \quad (33)$$

where T_2 is the kinetic energy of the flexible plate, M_i is the mass of the flexible plate, ρ_2 is the density of the flexible plate, V_2 is the volume of the flexible plate, and $\dot{r_p}$ is the velocity of an arbitrary point P.

Substitute Eq. (32) into Eq. (33), and we get Eq. (34):

$$T_2 = \frac{1}{2}\rho_2 h_2\iint_{A_2} a_1^2\dot{\theta}_1^2 + \dot{\theta}_2^2 x^2 + \dot{\theta}_2^2\emptyset_1^T\emptyset_1 q_1^2 + \dot{\theta}_2^2 H_1^2 q_3^4 + \emptyset_1^2\dot{q_1}^2 + H_1^2 q_3^2\dot{q_3}^2 + \dot{\theta}_2^2\emptyset_3^T\emptyset_3 q_3^2 + \emptyset_3^T\emptyset_3\dot{q_3}^2 + 2a_1\dot{\theta}_1\dot{\theta}_2 x\cos(\theta_1 - \theta_2) + 2a_1\dot{\theta}_1\dot{\theta}_2\emptyset_1 q_1\cos(\theta_1 - \theta_2) + 2a_1\dot{\theta}_1\dot{\theta}_2 H_1 q_3^2\cos(\theta_1 - \theta_2) + 2a_1\dot{\theta}_1\emptyset_1\dot{q_1}\sin(\theta_2 - \theta_1) + 2a_1\dot{\theta}_1 H_1 q_3\dot{q_3}\sin(\theta_2 - \theta_1) + 2a_1\dot{\theta}_1\dot{\theta}_2\emptyset_3 q_3\sin(\theta_1 - \theta_2) + 2a_1\dot{\theta}_1\emptyset_3\dot{q_3}\cos(\theta_1 - \theta_2) + 2\dot{\theta}_2^2 x\emptyset_1 q_1 + 2\dot{\theta}_2^2 x H_1 q_3^2 + 2\dot{\theta}_2 x\emptyset_3\dot{q_3} + 2\dot{\theta}_2^2\emptyset_1 q_1 H_1 q_3^2 + 2\dot{\theta}_2\emptyset_1 q_1\emptyset_3\dot{q_3} + 2\dot{\theta}_2 H_1 q_3^2\emptyset_3\dot{q_3} + 2\emptyset_1\dot{q_1}H_1 q_3\dot{q_3} - 2\emptyset_1\dot{q_1}\dot{\theta}_2\emptyset_3 q_3 - 2H_1 q_3^2\dot{q_3}\dot{\theta}_2\emptyset_3 + {\emptyset_2}^T\emptyset_2{\dot{q}_2}^2 + 4{H_2}^2{q_3}^2{\dot{q}_3}^2 + 4\emptyset_2\dot{q_2}H_2 q_3\dot{q_3}dA_2 \quad (34)$$

The calculation equation for the potential energy generated by the flexible plate is as follows in Eq. (35).

$$U_2 = \frac{1}{2}\iiint_{V_2}(\sigma_{xx}\varepsilon_{xx} + \sigma_{yy}\varepsilon_{yy} + \tau_{xy}\gamma_{xy})\mathrm{d}V_2 \quad (35)$$

Discretizing the strain and stress of the flexible plate structure yields

$$\sigma_{xx} = -\frac{E}{1-\mu^2}\left(\emptyset_{1,x}q_1 - z\emptyset_{3,xx}q_3 + \mu\emptyset_{2,y}q_2 - z\mu\emptyset_{3,yy}q_3\right);$$

$$\varepsilon_{xx} = \emptyset_{1,x}q_1 - z\emptyset_{3,xx}q_3 \quad (36)$$

$$\sigma_{yy} = -\frac{E}{1-\mu^2}\left(\emptyset_{2,y}q_2 - z\emptyset_{3,yy}q_3 + \mu\emptyset_{1,x} - z\mu\emptyset_{3,xx}q_3\right) \quad ;$$

$$\varepsilon_{yy} = \emptyset_{2,y}q_2 - z\emptyset_{3,yy}q_3 \quad (37)$$

$$\tau_{xy} = \frac{E}{2(1+\mu)}\left(\emptyset_{2,x}q_2 + \emptyset_{1,y}q_1 - 2z\emptyset_{3,x}\emptyset_{3,y}{q_3}^2\right) \quad ; \quad \gamma_{xy} = \emptyset_{2,x}q_2 + \emptyset_{1,y}q_1 - 2z\emptyset_{3,x}\emptyset_{3,y}{q_3}^2 \quad (38)$$

Substitute Eqs. (36) - (38) into Eq. (35), and we get Eq. (39):

$$U_2 = \frac{h_2 E}{2(\mu^2-1)}\iint_{A_2}\left(\emptyset_{1,x}^T\emptyset_{1,x}{q_1}^2 + \emptyset_{2,y}^T\emptyset_{2,y}{q_2}^2 - 2h\emptyset_{1,x}q_1\emptyset_{3,xx}q_3 - 2h\emptyset_{2,y}q_2\emptyset_{3,yy}q_3 + h^2\emptyset_{3,xx}^T\emptyset_{3,xx}{q_3}^2 + h^2\emptyset_{3,yy}^T\emptyset_{3,yy}{q_3}^2 + 2\mu\emptyset_{1,x}q_1\emptyset_{2,y}q_2 - 2h\mu\emptyset_{1,x}q_1\emptyset_{3,yy}q_3 - 2h\mu\emptyset_{2,y}q_2\emptyset_{3,xx}q_3 + 2h^2\mu\emptyset_{3,xx}q_3\emptyset_{3,yy}q_3\right)dA_2 + \frac{h_2 E}{4(1+\mu)}\iint_A\left(\emptyset_{2,x}^T\emptyset_{2,x}q_2^2 + \emptyset_{1,y}^T\emptyset_{1,y}q_1^2 + 4h^2\emptyset_{3,x}^T\emptyset_{3,x}\emptyset_{3,y}^T\emptyset_{3,y}q_3^4 + 2{\emptyset_{2,x}}^T\emptyset_{1,y}q_2q_1 - 4h{\emptyset_{1,y}}^T\emptyset_{3,x}\emptyset_{3,y}{}^Tq_1q_3^2 - 4h{\emptyset_{3,x}}^T\emptyset_{3,y}\emptyset_{2,x}{}^Tq_3^2q_2\right)dA_2 \quad (39)$$

Since the center of mass of the flexible plate is located at the geometric center of the plate, the gravitational potential energy of the flexible plate structure is solved as follows Eq. (40):

$$U_3 = \frac{1}{2}M_2 g(a_2 sin\theta_2 + a_1 sin\theta_1) = \frac{1}{2}a_2 b_2 h_2\rho_2 g(a_2 sin\theta_2 + a_1 sin\theta_1) \quad (40)$$

The kinetic energy and potential energy of the rigid-body-flexible-body coupling system are as shown in Eqs. (41) and (42).

$$U = U_1 + U_2 + U_3; \quad (42)$$

$$T = T_1 + T_2 \quad (42)$$

The Lagrange equation of the rigid-flexible coupling system in this study is as follows:

$$\frac{d}{dt}\left(\frac{\partial T}{\partial\dot{\theta}_1}\right) - \frac{\partial T}{\partial\theta_1} + \frac{\partial U}{\partial\theta_1} = \tau_1 - \tau_2 \quad (43)$$

$$\frac{d}{dt}\left(\frac{\partial T}{\partial\dot{\theta}_2}\right) - \frac{\partial T}{\partial\theta_2} + \frac{\partial U}{\partial\theta_2} = \tau_2 \quad (44)$$

$$\frac{d}{dt}\left(\frac{\partial T}{\partial\dot{q}_1}\right) - \frac{\partial T}{\partial q_1} + \frac{\partial U}{\partial q_1} = 0 \quad (45)$$

$$\frac{d}{dt}\left(\frac{\partial T}{\partial\dot{q}_2}\right) - \frac{\partial T}{\partial q_2} + \frac{\partial U}{\partial q_2} = 0 \quad (46)$$

$$\frac{d}{dt}\left(\frac{\partial T}{\partial\dot{q}_3}\right) - \frac{\partial T}{\partial q_3} + \frac{\partial U}{\partial q_3} = psin(\Omega t) \quad (47)$$

Substitute the kinetic energy and potential energy of the rigid-flexible coupling system into the Lagrange equation, and substitute Eqs. (1), (3), (34), (39), and (40) into Eqs. (43)-(47).

$$\begin{bmatrix} M_{\theta_1} & M_{\theta_1\theta_2} & M_{\theta_1 q_1} & M_{\theta_1 q_2} & M_{\theta_1 q_3} \\ M_{\theta_2\theta_1} & M_{\theta_2} & M_{\theta_2 q_1} & M_{\theta_2 q_2} & M_{\theta_2 q_3} \\ M_{q_1\theta_1} & M_{q_1\theta_2} & M_{q_1} & M_{q_1 q_2} & M_{q_1 q_3} \\ M_{q_2\theta_1} & M_{q_2\theta_2} & M_{q_2 q_2 q} & M_{q_2} & M_{q_2 q_3} \\ M_{q_3\theta_1} & M_{q_3\theta_2} & M_{q_3 q_1} & M_{q_3 q_2} & M_{q_3} \end{bmatrix} \begin{bmatrix} \ddot{\theta}_1 \\ \ddot{\theta}_2 \\ \ddot{q}_1 \\ \ddot{q}_2 \\ \ddot{q}_3 \end{bmatrix} + \begin{bmatrix} 0 & 0 & 0 & 0 & 0 \\ 0 & 0 & 0 & 0 & 0 \\ 0 & 0 & 0 & G_{q_1 q_2} & G_{q_1 q_3} \\ 0 & 0 & G_{q_2 q_2 q} & 0 & G_{q_2 q_3} \\ 0 & 0 & G_{q_3 q_1} & G_{q_3 q_2} & 0 \end{bmatrix} \begin{bmatrix} \dot{\theta}_1 \\ \dot{\theta}_2 \\ \dot{q}_1 \\ \dot{q}_2 \\ \dot{q}_3 \end{bmatrix} + \begin{bmatrix} 0 & 0 & 0 & 0 & 0 \\ 0 & 0 & 0 & 0 & 0 \\ 0 & 0 & K_{q_1} & K_{q_1 q_2} & K_{q_1 q_3} \\ 0 & 0 & K_{q_2 q_2} & K_{q_2} & K_{q_2 q_3} \\ 0 & 0 & K_{q_3 q_1} & K_{q_3 q_2} & K_{q_3} \end{bmatrix} \begin{bmatrix} \theta_1 \\ \theta_2 \\ q_1 \\ q_2 \\ q_3 \end{bmatrix} +$$

$$\begin{bmatrix} h_1 \\ h_2 \\ h_3 \\ h_4 \\ h_5 \end{bmatrix} = \begin{bmatrix} \tau_1 \\ \tau_2 \\ 0 \\ 0 \\ psin(\Omega t) \end{bmatrix} \tag{48}$$

$$\begin{bmatrix} M_{q_1} & M_{q_1 q_2} & M_{q_1 q_3} \\ M_{q_2 q_1} & M_{q_2} & M_{q_2 q_3} \\ M_{q_3 q_1} & M_{q_3 q_2} & M_{q_3} \end{bmatrix} \begin{bmatrix} \ddot{q}_1 \\ \ddot{q}_2 \\ \ddot{q}_3 \end{bmatrix} + \begin{bmatrix} 0 & G_{q_1 q_2} & G_{q_1 q_3} \\ G_{q_2 q_1} & 0 & G_{q_2 q_3} \\ G_{q_3 q_1} & G_{q_3 q_2} & 0 \end{bmatrix} \begin{bmatrix} \dot{q}_1 \\ \dot{q}_2 \\ \dot{q}_3 \end{bmatrix} + \begin{bmatrix} K_{q_1} & K_{q_1 q_2} & K_{q_1 q_3} \\ K_{q_2 q_1} & K_{q_2} & K_{q_2 q_3} \\ K_{q_3 q_1} & K_{q_3 q_2} & K_{q_3} \end{bmatrix} \begin{bmatrix} q_1 \\ q_2 \\ q_3 \end{bmatrix} + \begin{bmatrix} h_3 \\ h_4 \\ h_5 \end{bmatrix} = \begin{bmatrix} 0 \\ 0 \\ psin(\Omega t) \end{bmatrix} \tag{49}$$

$M_{q_1} = D_{11}$; $M_{q_1 q_2} = 0$; $M_{q_1 q_3} = C_{11} q_3$; $M_{q_2 q_1} = 0$; $M_{q_2} = D_{22}$; $M_{q_2 q_3} = 2C_{22} q_3$;

$M_{q_3 q_1} = C_{11} q_3$; $M_{q_3 q_2} = 2C_{22} q_3$; $M_{q_3} = I_{11} q_3^2 + D_{33} + D_{13} q_1 \dot{\theta}_2 + 4I_{22} q_3^2$;

$M_{q_1\theta_1} = a_1 A_1 \sin(\theta_2 - \theta_1)$; $M_{q_1\theta_2} = -D_{13} q_3$; $M_{q_2\theta_1} = 0$; $M_{q_2\theta_2} = 0$;

$M_{q_3\theta_1} = a_1 q_3 \sin(\theta_2 - \theta_1) J_1 + a_1 \cos(\theta_1 - \theta_2) A_3$; $M_{q_3\theta_2} = \mathrm{D}_{13} q_1 \dot{q}_3$

$G_{q_1 q_3} = -2D_{13} \dot{\theta}_2$; $G_{q_3 q_1} = D_{13} \dot{\theta}_2$

$K_{q_1} = \iint_{A_2} \left(N_1 \emptyset_{1,x}{}^T \emptyset_{1,x} - N_1 N_2 \emptyset_{1,y}{}^T \emptyset_{1,y} \right) dA_2$;

$K_{q_1 q_2} = \iint_{A_2} \left(N_1 \mu \emptyset_{1,x}{}^T \emptyset_{2,y} + N_1 N_2 \emptyset_{2,x}{}^T \emptyset_{1,y} \right) dA_2$;

$K_{q_1 q_3} = \iint_{A_2} \left(-N_1 h_2 \emptyset_{1,x}{}^T \emptyset_{3,xx} - N_1 h_2 \mu \emptyset_{1,x}{}^T \emptyset_{3,yy} \right) dA_2$;

$K_{q_2 q_1} = \iint_{A_2} \left(N_1 \mu \emptyset_{1,x}{}^T \emptyset_{2,y} + N_1 N_2 \emptyset_{2,x}{}^T \emptyset_{1,y} \right) dA_2$;

$K_{q_2} = \iint_{A_2} \left(N_1 \emptyset_{2,y}^T \emptyset_{2,y} + N_1 N_2 \emptyset_{2,x}^T \emptyset_{2,x} \right) dA_2$;

$K_{q_2 q_3} = \iint_{A_2} \left(-N_1 h_2 \emptyset_{2,y} \emptyset_{3,yy} - N_1 h_2 \mu \emptyset_{2,y} \emptyset_{3,xx} \right) dA_2$;

$K_{q_3 q_1} = \iint_{A_2} \left(-N_1\, h_2 \emptyset_{1,x}{}^T \emptyset_{3,xx} - N_1\, h_2 \mu \emptyset_{1,x}{}^T \emptyset_{3,yy} \right) dA_2$;

$K_{q_3 q_2} = \iint_{A_2} \left(-N_1 h_2 \emptyset_{2,y} \emptyset_{3,yy} - N_1 h_2 \mu \emptyset_{2,y} \emptyset_{3,xx} \right) dA_2$;

$$K_{q_3} = \iint_{A_2} \left(N_1 h_2{}^2 \emptyset_{3,xx}{}^T \emptyset_{3,xx} + N_1 h_2{}^2 \emptyset_{3,yy}{}^T \emptyset_{3,yy} + 2N_1 h_2{}^2 \mu \emptyset_{3,xx}{}^T \emptyset_{3,yy} \right) dA_2 + 2C_{31} \dot{q}_3 \dot{\theta}_2 - 9I_{11} \dot{q}_3^2 + 2I_{11} q_3^2 \dot{\theta}_2^2 + D_{33} \dot{\theta}_2^2 + 2L_1 \dot{\theta}_2^2 + 4I_{22} \dot{q}_3{}^2 - 8N_1 N_2 Q q_3^2;$$

$h_3 = -a_1 \cos(\theta_2 - \theta_1)\, \dot{\theta}_1^2 A_1 + a_1 \cos(\theta_2 - \theta_1)\, \dot{\theta}_1 \dot{\theta}_2 A_1 + C_{11} \dot{q}_3{}^2 - D_{11} q_1 \dot{\theta}_2^2 - a_1 A_1 \cos(\theta_1 - \theta_2)\, \dot{\theta}_1 \dot{\theta}_2 - B_{x1} \dot{\theta}_2^2 - C_{11} q_3^2 \dot{\theta}_2^2 - 2N_1 N_2 W_1 q_3^2 + M_{q_1\theta_1} \ddot{\theta}_1 + M_{q_1\theta_2} \ddot{\theta}_2$;

$h_4 = 2C_{22} \dot{q}_3{}^2 - 2N_1 N_2 W_2 q_3^2 + M_{q_2\theta_1} \ddot{\theta}_1 + M_{q_2\theta_2} \ddot{\theta}_2$;

$h_5 = a_1 J_1 \sin(\theta_2 - \theta_1)\, \dot{\theta}_1 \dot{q}_3 - a_1 J_1 \cos(\theta_2 - \theta_1)\, q_3 \dot{\theta}_1^2 + a_1 J_1 \cos(\theta_2 - \theta_1) q_3 \dot{\theta}_1 \dot{\theta}_2 - a_1 A_3 \sin(\theta_1 - \theta_2)\, \dot{\theta}_1^2 + a_1 A_3 \sin(\theta_1 - \theta_2)\, \dot{\theta}_1 \dot{\theta}_2 + 2C_{31} \dot{\theta}_2 \dot{q}_3{}^2 - 2a_1 J_1 \cos(\theta_1 - \theta_2) q_3\, \dot{\theta}_1 \dot{\theta}_2 - a_1 J_1 \sin(\theta_2 - \theta_1)\, \dot{\theta}_1 \dot{q}_3 - a_1 \mathrm{A}_3 \sin(\theta_1 - \theta_2)\, \dot{\theta}_1 \dot{\theta}_2 - 2C_{11} q_1 q_3 \dot{\theta}_2^2 + 4C_{22} \dot{q}_2 \dot{q}_3 - 4N_1 N_2 R q_1 q_3 - 4N_1 N_2 q_3 q_2 + M_{q_3\theta_1} \ddot{\theta}_1 + M_{q_3\theta_2} \ddot{\theta}_2$;

Note:

$A_i = \iint_{A_2} \rho_2 h_2 \phi_i dA_2$; $B_{xi} = \iint_{A_2} \rho_2 h_2 x \emptyset_i dA_2$; $C_{ij} = \iint_{A_2} \rho_2 h_2 \emptyset_i H_j dA_2$;

$D_{ij} = \iint_{A_2} \rho_2 h_2 \emptyset_i{}^T \emptyset_j dA_2$; $N_1 = \frac{h_2 E cos\theta_2}{(\mu^2-1)}$; $N_2 = \frac{\mu-1}{2}$; $W_1 = \iint_{A_2} h_2 \emptyset_{1,y}{}^T \emptyset_{3,x} \emptyset_{3,y}{}^T dA_2$;

$W_2 = \iint_{A_2} h_2 \emptyset_{3,x}{}^T \emptyset_{3,y} \emptyset_{2,x}{}^T dA_2$; $I_{ij} = \iint_{A_2} \rho_2 h_2 \mathrm{H}_i{}^T \mathrm{H}_j dA_2$; $J_i = \iint_{A_2} \rho_2 h_2 \mathrm{H}_i dA_2$;

$L_i = \iint_{A_2} \rho_2 h_2 x \mathrm{H}_i dA_2$; $Q = \iint_{A_2} h_2{}^2 \emptyset_{3,x}^T \emptyset_{3,x} \emptyset_{3,y}^T \emptyset_{3,y} dA_2$;

$R = \iint_{A_2} h_2{}^2 \emptyset_{1,y}{}^T \emptyset_{3,x} \emptyset_{3,y}{}^T dA_2$; $S = \iint_{A_2} h_2{}^2 \emptyset_{3,x}{}^T \emptyset_{3,y} \emptyset_{2,x}{}^T dA_2$.

where M_{θ_1} and M_{θ_2} are the moments of inertia of the rigid plate structure and the flexible plate structure system respectively. $M_{q_i q_j}$ $(i = 1,2;\ j = 1,2)$ is an $N \times N$ dimensional generalized mass matrix, and the truncation order of the model vibration modes is N. $M_{\theta_i q_j} \in R^{1\times N}$ $(i = 1,2;\ j = 1,2)$ represents the nonlinear coupling term between the large-range rotational motion and the flexible deformation of the flexible plate structure. $G_{q_i q_j}$ $(i = 1,2;\ j = 1,2)$ reflects the gyroscopic effect of the system, and all are $N \times N$ dimensional matrices. $K_{q_i q_j}$ $(i = 1,2;\ j = 1,2)$ is the stiffness of the system, and all are $N \times N$ dimensional stiffness matrices. τ_1 and τ_2 are the driving torques relative to θ_1 and θ_2. H_i is the nonlinear term of the dynamic equation of the rigid-flexible coupling system. p is the amplitude of the external excitation, and Ω is the circular frequency of the external excitation.

For the case where the large range motion of the rigid-flexible coupling system is known, the angular displacement, angular velocity, and angular acceleration are all known and do not need to be solved. Moreover, there is no influence of the input of the control equation at this time. Therefore, by organizing Eq. (48), the nonlinear dynamic equation of the rigid-flexible hybrid system is as follows in Eq. (49). Among them, the terms in the dynamic equation that contain C_{ij}, I_{ij}, J_i and L_i are the coupling terms of the rigid-flexible coupling structure. The coupling terms represent the additional stiffness brought by the rigid-flexible coupling deformation. The dynamic equation with the coupling terms removed ignores the influence of the rigid-flexible coupling deformation on the structure.

3. Rigid-flexible coupling characteristic case analysis

Since the mode shape of the folded wing structure is extremely similar to that of the cantilever plate structure, the mode function of the cantilever beam is selected in the x-direction, and the mode function of the free-beam is selected in the y-direction. The mode functions in the x and y directions are combined to form the mode function of the cantilever plate. Under the condition of satisfying the displacement boundary conditions, the mode-shape functions of $\emptyset_1(x,y)$, $\emptyset_2(x,y)$ and $\emptyset_3(x,y)$ are assumed using Eqs. (50)-(58).

$$\emptyset_1(x,y) = \sin\frac{\pi}{2}x \cos\pi y - \sin\pi x \cos\frac{\pi}{2}y \tag{50}$$

$$\emptyset_2(x,y) = \cos\frac{\pi}{2}x \sin\pi y + \cos\pi x \sin\frac{\pi}{2}y \tag{51}$$

$$\emptyset_3(x,y) = X_1 * Y_1 + X_2 * Y_2 \tag{52}$$

$$X_i = \cosh k_i x - \cos k_i x - \alpha_i(\sinh k_i x - \sin k_i x) \tag{53}$$

$$\cos(k_i)\cosh(k_i) + 1 = 0 \tag{54}$$

$$\alpha_i = \frac{\sinh k_i - \sin k_i}{\cosh k_i + \cos k_i} \tag{55}$$

$$Y_i = \cosh l_i y + \cos l_i y - \beta_i(\sinh l_i y + \sin l_i y) \tag{56}$$

$$\cos(l_i)\cosh(l_i) - 1 = 0 \tag{57}$$

$$\beta_2 = \frac{\cosh(l_i) - \cos(l_i)}{\sinh(l_i) - \sin(l_i)} \tag{58}$$

The rigid-flexible coupling dynamic equation of the folded wing mainly takes into account the transverse vibration response of the structure. The dynamic equation of the transverse vibration of the system is as shown in Eqs. (59) and (60). The underlined polynomial in K_{q_3} is the additional stiffness brought about by the rigid-flexible coupling deformation.

$$M_{q_1}\ddot{q}_3 + K_{q_3} q_3 + h_5 = 0 \tag{59}$$

$$K_{q_3} = \iint_{A_2}\left(N_1 h_2{}^2 \emptyset_{3,xx}{}^T \emptyset_{3,xx} + N_1 h_2{}^2 \emptyset_{3,yy}{}^T \emptyset_{3,yy} + 2N_1 h_2{}^2 \mu \emptyset_{3,xx}{}^T \emptyset_{3,yy}\right) dA_2 + 2C_{31}\dot{q}_3\dot{\theta}_2 - 9I_{11}\dot{q}_3^2 + 2I_{11}q_3^2\dot{\theta}_2^2 + D_{33}\dot{\theta}_2^2 + 2L_1\dot{\theta}_2^2 + 4I_{22}\dot{q}_3{}^2 - 8N_1N_2Qq_3^2 \tag{60}$$

In the rigid-flexible coupling system, the width of the rigid inner wing plate $\mathrm{b}_1 = 0.4\mathrm{m}$, the density of the flexible plate structure $\rho_2 = 1600kg/m^3$, the thickness $h_2 = 0.002m$, the length of the outer wing plate $a_2 = 0.2m$, the elastic modulus of the flexible plate $E = 10e9pa$, and the Poisson's ratio $\mu = 0.3$. As can be seen from the rigid-flexible coupling dynamics equation, the coupling stiffness of the structure is independent

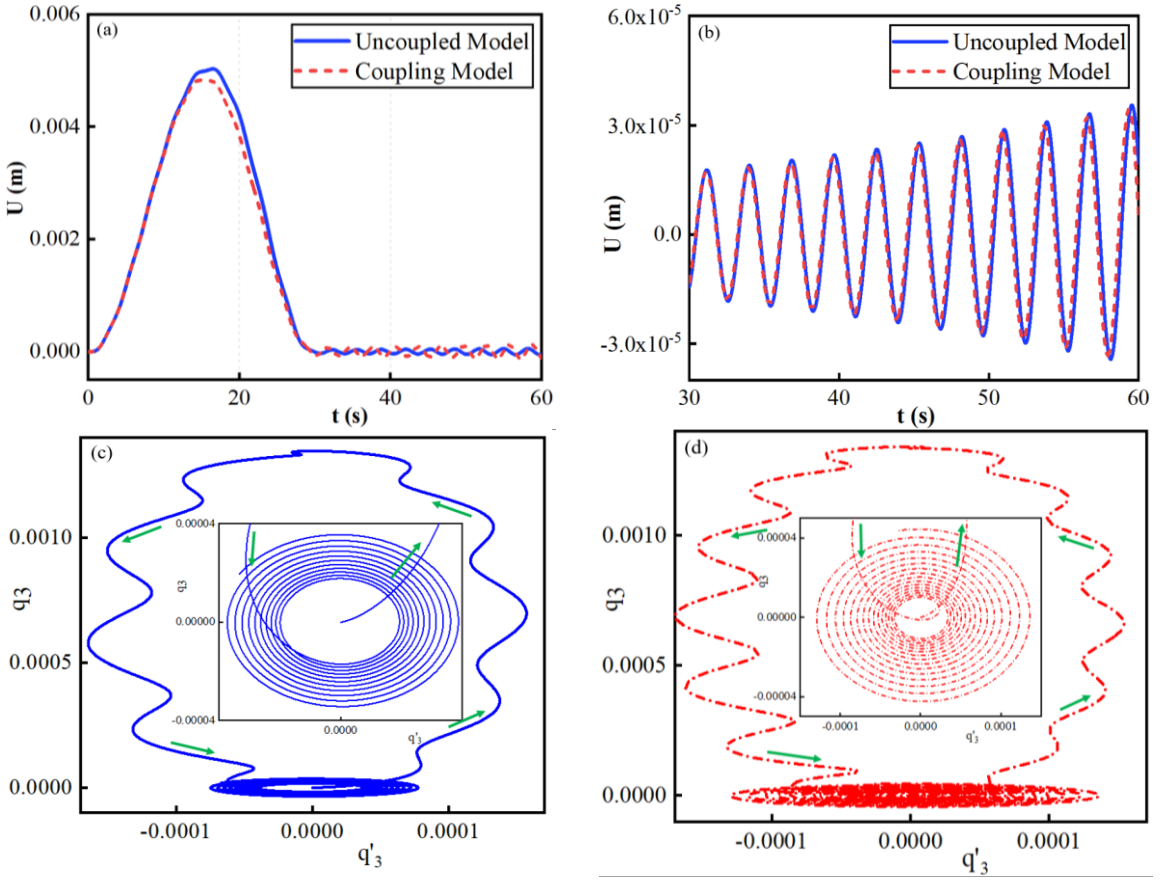

Fig. 2: The vibration response in the z-direction of the midpoint at the top of the model when $\omega = 0.1Hz$ (a) Time-domain response of the system, (b)Locally amplified time-domain response, (c) Velocity-Amplitude response of uncoupling model, and (d) Velocity-Amplitude response of coupling model.

of the rotational speed of the rigid structure. Therefore, the expression of the driving torque τ_2 of the flexible plate structure is assumed as follows Eq. (61):

$$\tau_2 = \begin{cases} 0.04sin\,(\omega t), 0 \le t \le 30 \\ 0, t > 30 \end{cases} \quad (61)$$

Select the circular frequency of the driving torque ω of the flexible outer wing as the control parameter. Based on the dynamic equation of the rigid-flexible coupling structure of the folded wing, use MATLAB software to perform numerical calculations on the system, and obtain the analysis of the transverse vibration response of the structure under different driving circular frequencies as shown in Figs. 2-5.

Fig. 2 shows the vibration response signals in the z-direction of the midpoint at the top of the model for the rigid-flexible coupling dynamics model and the uncoupling stiffness structure dynamics model of the folded wing when the system rotation frequency is $\omega = 0.5Hz$. Fig. 2(b) is a local time-domain response enlarged view of Fig. 2(a) from 30s-60s, and it is also the time-domain response signal of the structure's steady-state vibration. As can be seen from Figs. 2(a) and (b), when the system rotation frequency is $\omega = 0.5Hz$, the time-domain response differences between the rigid-flexible coupling model and the uncoupling model in the z-direction are small, and the amplitudes and frequencies at the trigonometric functions are also very close. Figs. 2(c) and (d) show the relationship between velocity and displacement responses. The data shows that after an unstable vibration transition period, the structure enters the steady-state response stage. Compared with the uncoupling model, the response amplitude and vibration trend of the rigid-flexible coupling model are basically consistent.

Fig. 3 shows the vibration response signals in the z-direction of the midpoint at the top of the model for the rigid-flexible coupling dynamics model and the uncoupling stiffness structure dynamics model of the folded wing when the system rotation frequency is $\omega = 0.5Hz$. Fig. 3(b) is a local time-domain response enlarged view of Fig. 3(a) from 30s-60s, and it is also the time-domain response signal of the structure's steady-state vibration. The time-domain signals in Figs. 3(a) and 3(b) show that the amplitude of the uncoupling dynamics model is slightly larger than that of the rigid-flexible coupling model. Compared with Fig. 2, as the frequency of the driving torque increases, the amplitude of the time-domain signal

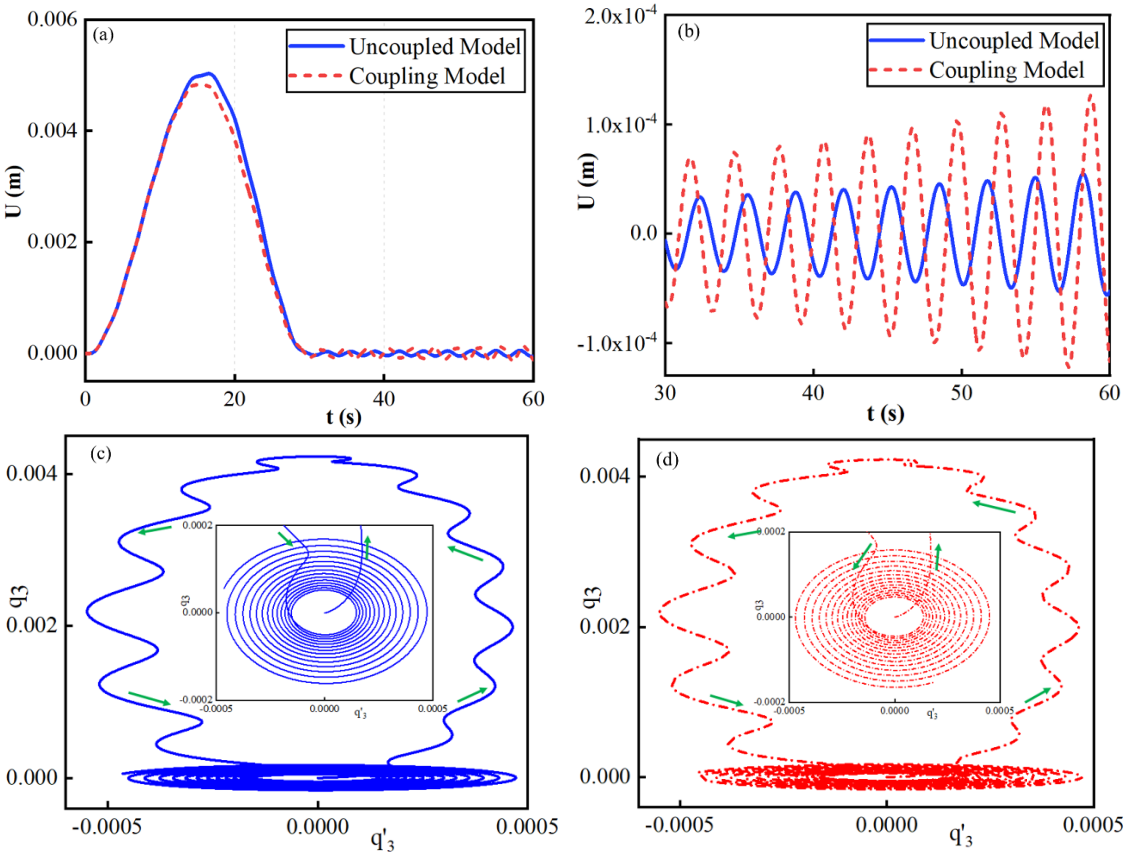

Fig. 3: The vibration response in the z-direction of the midpoint at the top of the model when $\omega = 0.5Hz$ (a) Time-domain response of the system, (b) Locally amplified time-domain response, (c) Velocity-Amplitude response of uncoupling model, and (d) Velocity-Amplitude response of coupling model.

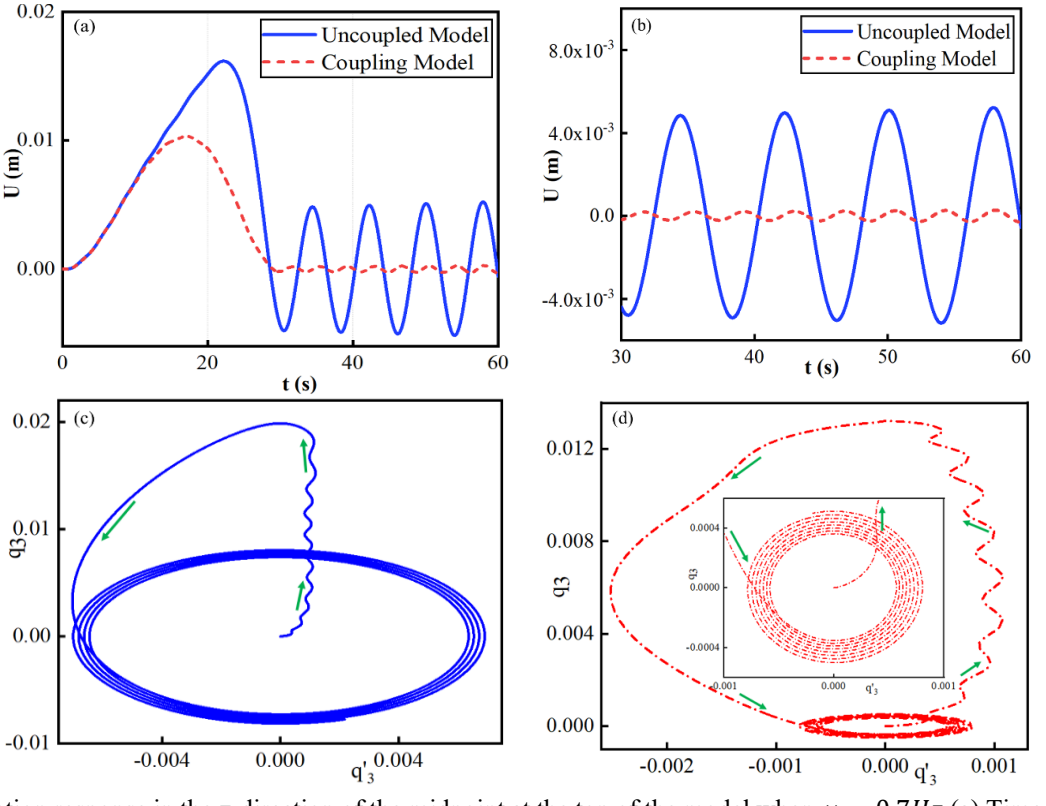

Fig. 4: The vibration response in the z-direction of the midpoint at the top of the model when $\omega = 0.7Hz$ (a) Time-domain response of the system, (b) Locally amplified time-domain response, (c) Velocity-Amplitude response of uncoupling model, and (d) Velocity-Amplitude response of coupling model.

more than doubles. Figs. 3(c) and 3(d) show the relationship between the velocity and displacement responses of the model. The data shows that after an unstable vibration transition period, the structure enters the steady-state response stage. Compared with the uncoupling model, the response amplitude and vibration trend of the rigid-flexible coupling model are basically consistent, and the vibration response trend of the structure is the same as that in Fig. 2.

Fig. 4 shows the vibration response signals in the z-direction of the midpoint at the top of the model for the rigid-flexible coupling dynamics model and the uncoupling stiffness structure dynamics model of the folded wing when the system rotation frequency is $\omega = 0.7Hz$. Fig. 4(b) is a local time-domain response enlarged view of Fig. 4(a) from 30s - 60s, and it is also the time-domain response signal of the structure's steady-state vibration. The time-domain amplitude response of the structure is significantly larger compared to that in Fig. 2 and Fig. 3. The amplitude of the rigid-flexible coupling model after stabilization is much smaller than that of the uncoupling model. Figs. 3(c) and (d) show the relationship between the velocity and displacement responses of the model. The data shows that after an unstable vibration transition period, the structure enters the steady-state response stage. Fig. 3 shows that the vibration response of the uncoupling model is significantly greater than that of the rigid-flexible coupling model. During the vibration transition stage, the amplitude of the uncoupling model exhibits an excitation phenomenon and then returns to steady-state vibration.

Fig. 5 shows the vibration response signals in the z-direction of the midpoint at the top of the model for the rigid-flexible coupling dynamics model and the uncoupling stiffness structure dynamics model of the folded wing when the system rotation frequency is $\omega = 0.8Hz$. When the frequency of the angular velocity increases to $0.8Hz$, the time-domain amplitude of the non-rigid-flexible coupling system shows a divergence phenomenon, while the vibration trend of the time-domain response signal of the rigid-flexible coupling system basically remains unchanged. After an unstable vibration transition period, the structure enters the steady-state response stage. The relationship between velocity and displacement responses shown in Figs. 3(b) and (c) indicates that the uncoupling model does not have a steady-state vibration and diverges directly, while the rigid-flexible coupling model still enters the steady-state response stage after an unstable

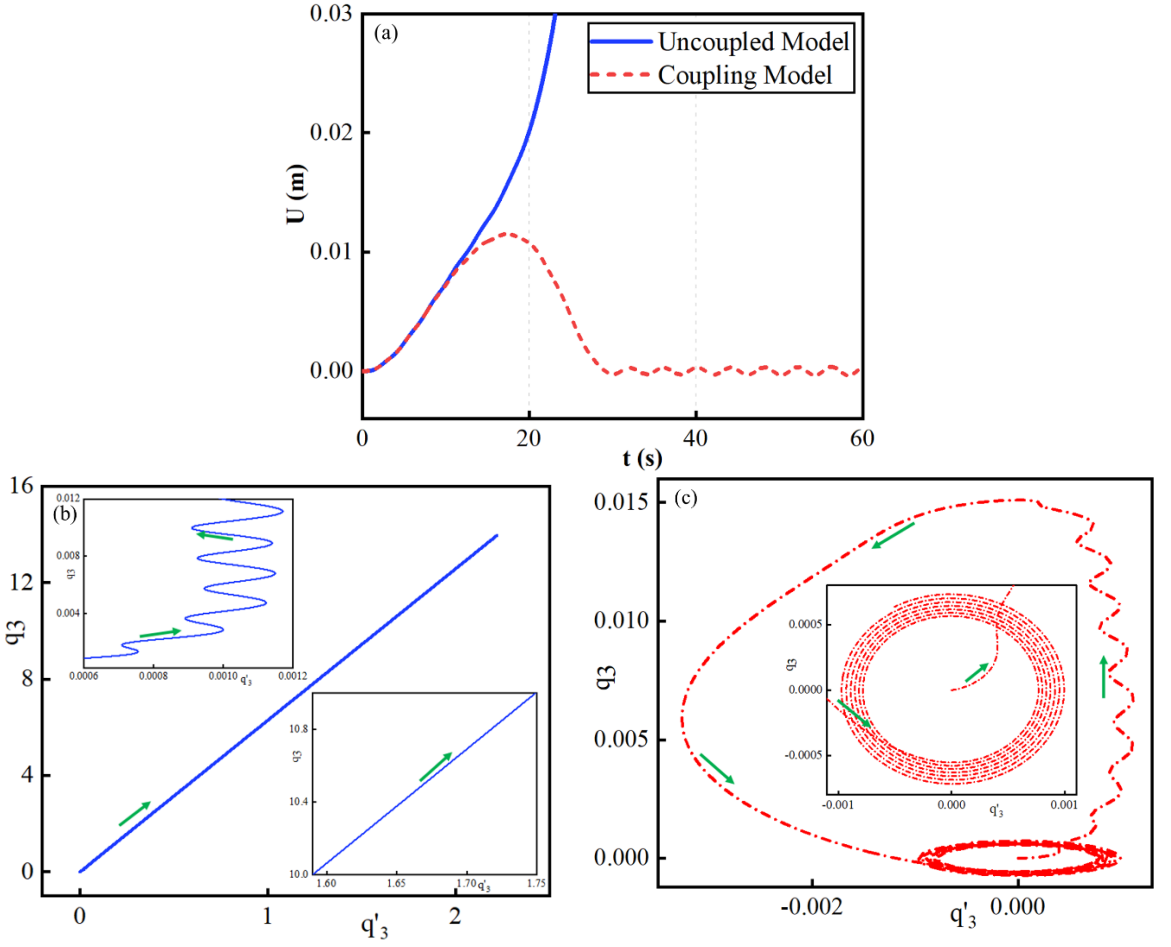

Fig. 5: The vibration response in the z-direction of the midpoint at the top of the model when $\omega = 0.8Hz$ (a) Time-domain response of the system, (b) Velocity -Amplitude response of uncoupling model, and (c) Velocity -Amplitude response of coupling model.

vibration transition period.

As comprehensively shown in Figs. 2-4, as the frequency of the driving torque increases, the vibration responses of the folded wing dynamics system gradually increase. The time-domain amplitude of the non-rigid-flexible coupling system gradually becomes much larger until divergence occurs finally. However, for the rigid-flexible coupling model, the vibration response increases slightly, and the overall vibration response trend remains unchanged. Based on the above calculation results, when the outer wing rotates under the action of torque, the additional stiffness brought by the rigid-flexible coupling deformation is more consistent with the structural dynamics model and motion law. To verify the accuracy of the rigid-flexible coupling dynamics model, the first two order vibration frequencies of the rigid-flexible coupling model are solved.

4. Case analysis of structural dynamic characteristics

4.1 Natural frequencies of the structure

The rigid-flexible coupling dynamics equation with coupling stiffness is more consistent with the actual situation of the structure. The dynamic characteristics of the rigid-flexible coupling dynamics model are further studied through the first two main vibration modes of the structure. For more realistic research, this section focuses on a thin-plate structure with a forward sweep angle $\chi_0 = 27°$ and an aft sweep angle $\chi_1 = -4°$. The wing chord length $b_1 = 0.8\text{m}$, the inner wingspan $a_1 = 0.4m$, the density of the flexible plate structure $\rho_2 = 1600\text{kg/m}^3$, the thickness $h_2 = 0.002\text{m}$, the outer wingspan $a_2 = 0.2m$, the elastic modulus of the flexible plate $E = 10e9pa$, and the Poisson's ratio $\mu = 0.3$. The finite element modeling and simulation calculation and the analytical analysis method of the dynamics equation are adopted to study the dynamic characteristics and variation laws of the folded wing structure.

Since the vibration frequency is an inherent property of the structure, and the structure needs to be solved in a stable state, the Folding angle θ_2 is solved in the states of 0°, 20°, and 40° respectively, with the small-disturbance angle θ_1 of the inner wing being a fixed angle. After truncating the first four order modes of the generalized coordinate vector $[q_1\ q_2\ q_3]^T$, the first four order modal dynamic equations of the structure are obtained. Substituting the mode-shape function and generalized coordinates into the dynamic equation (44), a two degree of freedom rigid-flexible coupling dynamic equation can be obtained. Based on the mass matrix, stiffness matrix, and damping matrix of the structure, the vibration frequencies of the folded wing structure under different Folding angles are solved. The first two order vibration frequencies of linear and nonlinear structures at different Folding angles are compared as shown in Table 1 and Fig. 6.

The data in Table 1 and Fig. 6 show that by comparing the three calculation methods, it can be seen that the solutions of the first four order natural frequencies of the structure by the nonlinear numerical model and the finite element model are very close, while the natural frequencies obtained by the linear numerical calculation method have relatively large differences after the third order mode. The nonlinear deformation caused by the large deformation of the folded wing structure has little effect on the first two order natural frequencies of the structure, but the calculation error gradually increases with the increase of the degrees of freedom of the structure. In addition, the natural frequencies of the folded wing in different Folding angle states are different, and there is no uniform variation law. For example, the first order natural frequency increases with the increase of the angle, while the second order natural frequency decreases with the increase of the angle.

Table 1: Vibration frequencies of folded wings at different folding angles.

Folding angles	Mode	Linear Numerical Calculation (Hz)	Nonlinear Numerical Calculation (Hz)	Finite Element Simulation (Hz)
0°	First	3.49	3.49	3.52
	Second	10.57	9.94	10.39
	Third	16.71	14.64	14.20
	Fourth	22.80	25.9	25.92
20°	First	3.52	3.53	3.58
	Second	10.51	9.80	10.01
	Third	15.90	14.05	13.52
	Fourth	22.10	25.11	25.00
40°	First	3.63	3.77	3.85
	Second	10.12	9.61	9.56
	Third Mode	15.76	12.75	12.20
	Fourth Mode	21.57	23.43	23.54

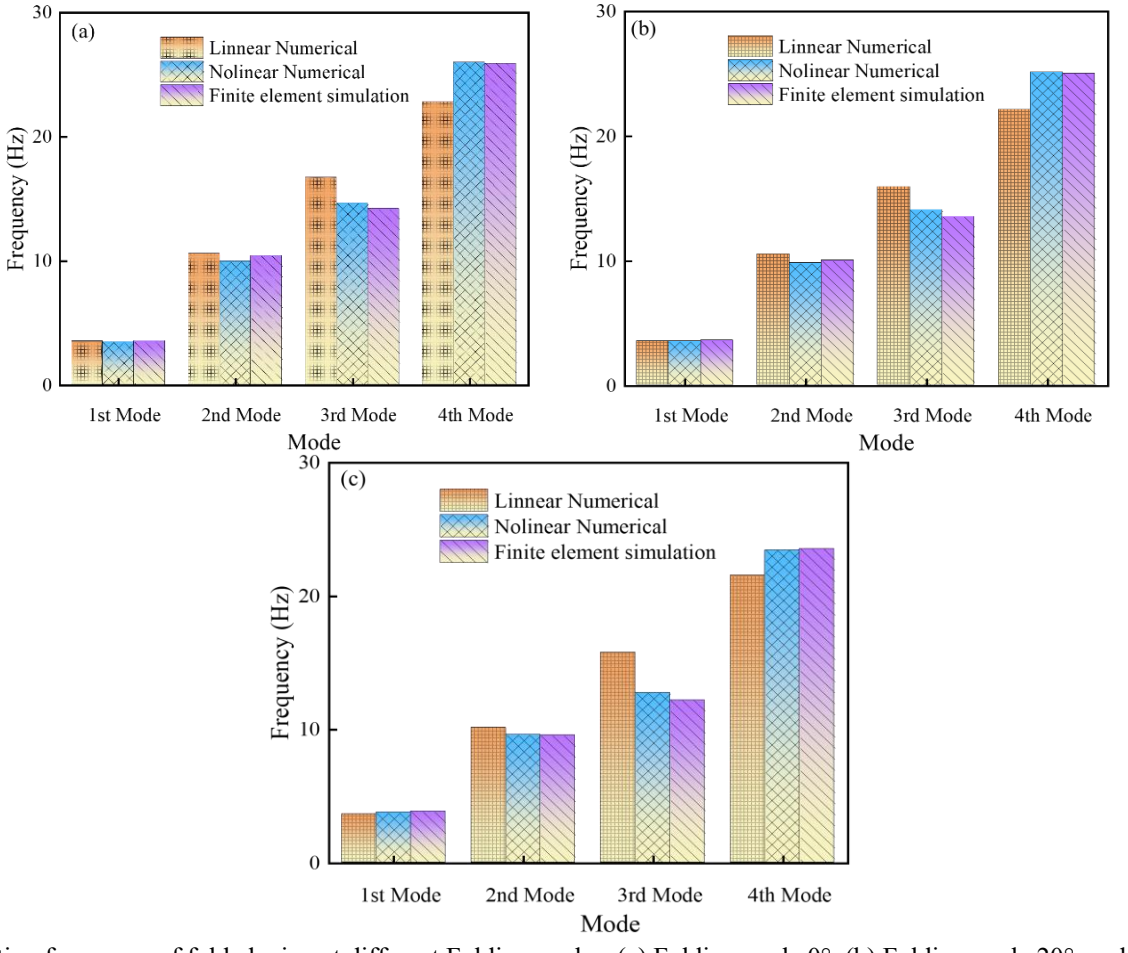

Fig. 6: Vibration frequency of folded wing at different Folding angles, (a) Folding angle 0°, (b) Folding angle 20°, and (c) Folding angle 40°.

4.2 Influence of transverse external excitation on system vibration characteristics

In this study, the transverse external excitation $psin(\Omega t)$ is selected as the control parameter. Based on the dynamic equation of the rigid - flexible coupling structure of the folded wing, MATLAB software is used to perform numerical calculations on linear and nonlinear structures to obtain the dynamic responses of the structures. In addition, a comparison is made with the dynamic responses obtained from finite element simulation calculations to analyze the differences in the results. It is assumed that the amplitude $p = 1$ and the excitation circular frequency $\Omega = 10Hz$, which is applied in the transverse direction (q_3 direction) of the model. First, the time-domain response results of numerical calculation and finite element simulation for the folded wing structure in the 0 Folding angle state are shown in Figs. 7-9.

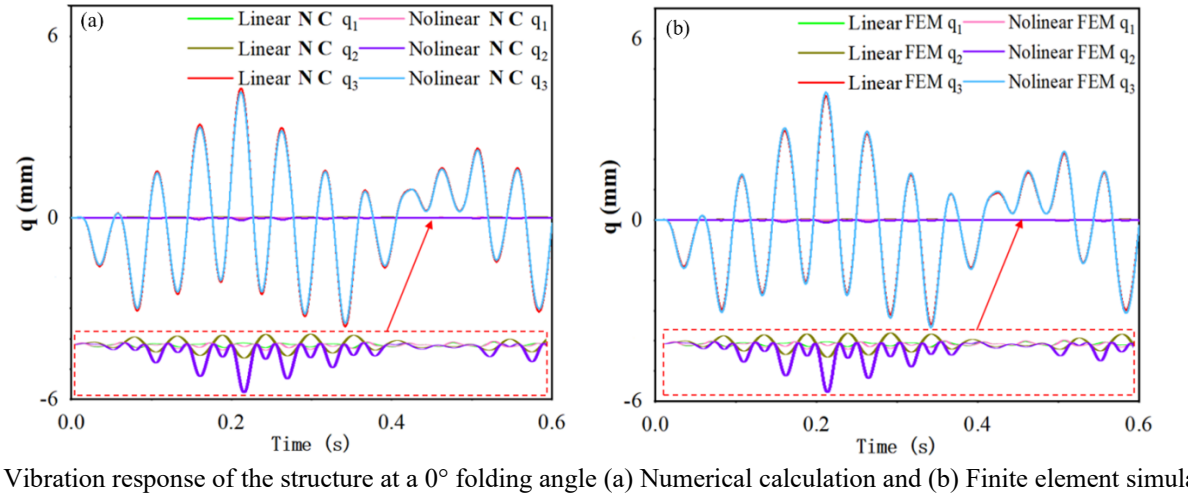

Fig. 7: Vibration response of the structure at a 0° folding angle (a) Numerical calculation and (b) Finite element simulation.

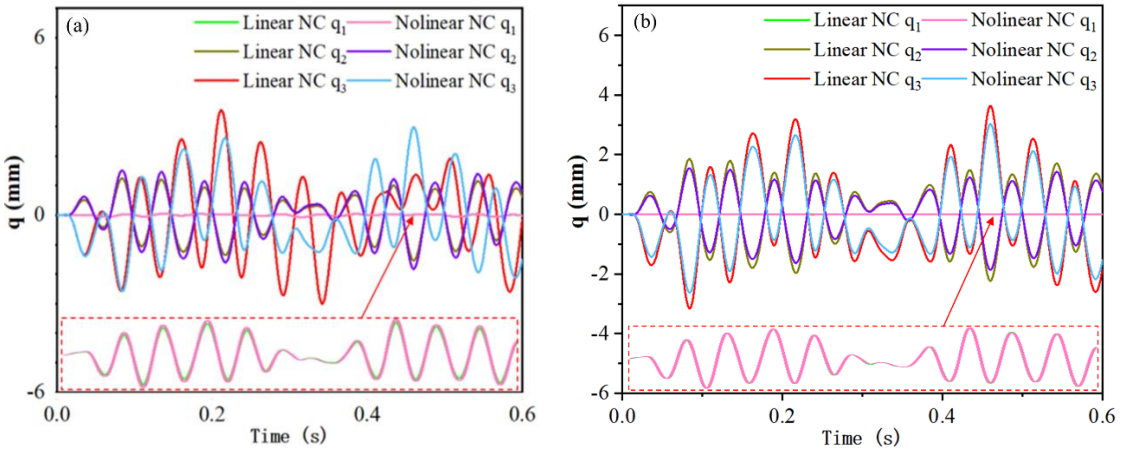

Fig. 8: Vibration response of the structure at a 20° folding angle (a) Numerical calculation, (b) Finite element simulation.

Fig. 7 shows the vibration response of the system to the transverse external excitation when the folded wing is at a 0° Folding angle. In the 0° Folding angle state, the effect of the transverse external excitation on the structure is mainly reflected in the q_3 direction, and the transverse vibration response is much larger than the vibration responses in the other two directions. The calculation results of the numerical method and the finite element method show that the time-domain amplitudes and frequency responses of the structure in the three directions are basically consistent. In addition, the nonlinearity of the structure has an insignificant effect on the time-domain response of the structure. The amplitude response has a slight change, and the nonlinear effect can be ignored.

Fig. 8 shows the vibration response of the system to the transverse external excitation when the folded wing is at a 20° folding angle. In the 20° folding angle state, the effect of the transverse external excitation on the structure is mainly reflected in the q_2 and q_3 directions, and the change in the vibration amplitude response in the q_1 direction is not significant. The calculation results show that the results of nonlinear numerical calculation and nonlinear finite element calculation are highly consistent, while the amplitude response of linear numerical calculation is on the large side. In addition, in the result of linear numerical calculation, around 0.3s, the amplitude response in the q_3 direction is greater than that in the q_2 direction, and this result is much larger than the results of finite element calculation and the nonlinear numerical solution, indicating that the linear numerical model has a large deviation.

Fig. 9 shows the vibration response of the system to the transverse external excitation when the folded wing is at a 40° Folding angle. In the 40° Folding angle state, the effect of the transverse external excitation on the structure is mainly reflected in the q_2 and q_3 directions. The amplitude in the q_3 direction is smaller than that in the q_2 direction, and the change in the vibration amplitude response in the q_1 direction is not significant. The calculation results show that the results of nonlinear numerical calculation and nonlinear finite element calculation are highly consistent, and the amplitude response of linear numerical calculation is on the small side.

The data in Figs. 7-9 show that the calculation results of the nonlinear numerical model are highly consistent with those

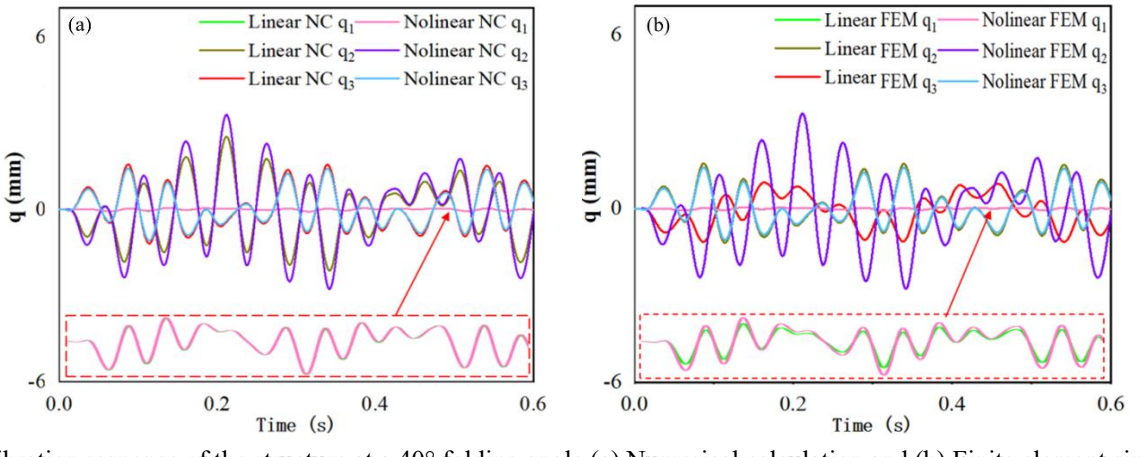

Fig. 9: Vibration response of the structure at a 40° folding angle (a) Numerical calculation and (b) Finite element simulation.

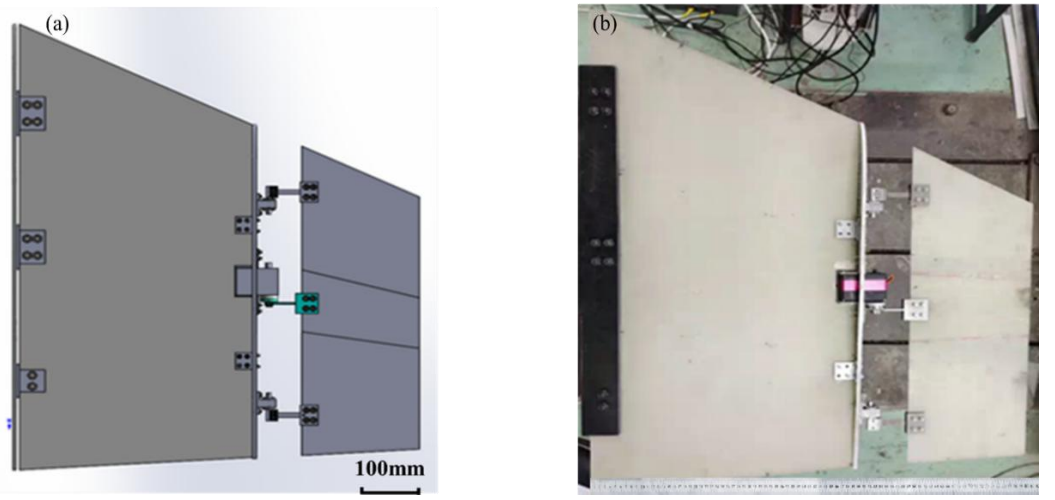

Fig. 10: Folded wing model (a) 3D structure of the folded wing and (b) Experimental model of the folded wing.

of the finite element method, which is in line with the vibration response characteristics. In the 0° Folding angle state, the vibration response of the structure calculated by the linear numerical model is similar to that of the nonlinear model. However, as the Folding angle increases, the deviation between the response of the linear numerical model and that of the nonlinear model becomes larger. The data of the finite element model show that there are slight differences between the calculation results of the linear finite element method and the nonlinear finite element method.

5. Experimental verification

5.1 Model experiment

An equivalent simplified model of the folded wing is manufactured based on the principles of functional and structural similarity, and structural dynamics tests are carried out to further verify the accuracy of the dynamic numerical model. The structural design and analysis method of the model are based on the basic equations of the structural mechanics of the folded wingtip. The focus is on restoring the principle of functional similarity of the folded wingtip, as well as the equivalent characteristics of the mass matrix and stiffness matrix of the structure. A folded - rotating wing model with a core plate as the base is manufactured. The model is divided into two parts: the inner wing and the outer wing. The root of the inner wing is supported by three solid support points at the base. In contrast, the outer wing can rotate around the rotary axis located between the inner and outer wings and is driven by a single - axis servo. The inner and outer wings are connected by three spring tabs; the intermediate spring tab is connected to the driven servo. The entire folded area is attached to the end rib of the inner wing, and the connector is fixed to it as well. The wings are fabricated from *2mm* thick glass fiber composite plates, which have an elastic modulus of *10GPa*, a poisson's ratio of 0.3, and a density of $1.6\times10^3\ kg/m^3$. A programmable logic controller (PLC) controls the steering gear, enabling the continuous angle change of the folding wing. The wing experimental model features a chord length of *800mm*, a span length of *800mm*, a forward sweep angle of 27°, and a backward sweep angle of -4°. The main material of the wing is a glass fibre composite panel structure. The composite panels are made of glass fibre cloth orthogonally laminated and bonded by a curing agent with a thickness of 0.1 mm. The 3D modeling and manufactured sample are shown in Fig. 10.

The main vibration modes of the structure are obtained through the ground experiment of the experimental model. The experimental model is fixedly installed on the experimental platform with the end face of the fixture root. Points representing geometric features are selected on the folded wing as the input of the model information. The hammering method is used to excite the model. The vibration signals of the model are collected by the acceleration sensors pasted on the surface of the model. The data collected by the signal acquisition card are transmitted to the computer processor. Finally, the post-processing software LMS Test Lab is used to process the data and fit to obtain the modal frequencies and vibration modes of the equivalent model. The experimental process of the model is shown in Fig. 11 below. For the model experiments, the sensors were placed at locations where the structural response was significant and therefore placed at the leading edge of the model. In addition, the data were collected five times for each structural feature point, and abnormal data were directly deleted when they appeared to ensure that the data obtained were highly accurate.

5.2 Experimental results and discussion

The hammering method is used to obtain the vibration modes and natural frequencies of the folded wing model at different

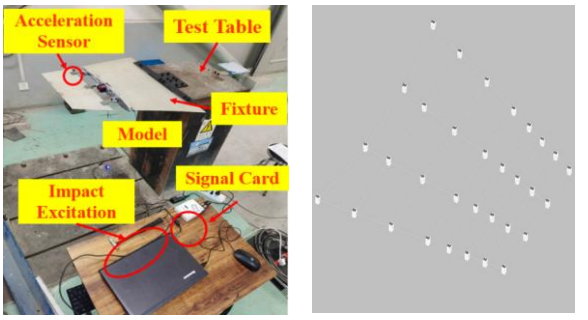

Fig. 11: Model experiment.

Folding angles. The results obtained by the numerical calculation and finite element simulation methods are compared with the experimental results. Since the vibration patterns of the folded wing model in different Folding angle states are similar, only the results at a 0° Folding angle are selected for comparison. The results are shown in Table 2.

Table 2 presents the vibration modes of the folded wing model obtained by different analysis methods. From the modal vibration mode diagrams, it can be seen that the vibration patterns of the folded wing obtained by different calculation methods are basically in agreement. The vibration modes of the first four orders of the folded wing are respectively the bending mode, the torsional mode, the secondary bending mode, and the secondary torsional mode. In order to more accurately demonstrate the dynamic characteristics of the structures solved by different methods, a precise comparison is made through the natural frequencies of the structures.

Fig. 12 shows the natural frequencies of the folded wing structure obtained by different research methods. The data shows that the first four-order natural frequencies of the structure solved by the finite-element model and the rigid-flexible coupling nonlinear dynamics equation are in high

Table 2: Vibration modes of the folded wing.

Mode	Numerical Calculation	Finite Element Simulation	Experiment
1	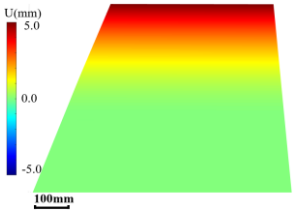	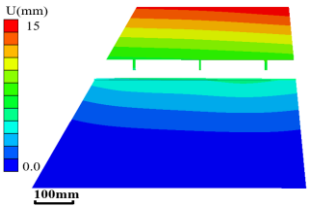	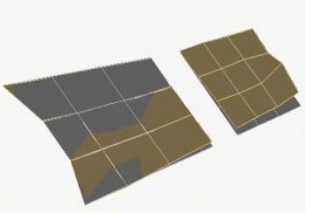
2	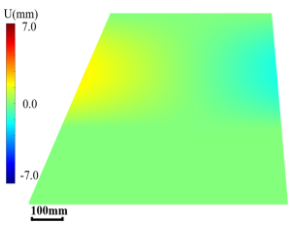	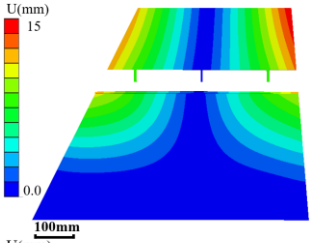	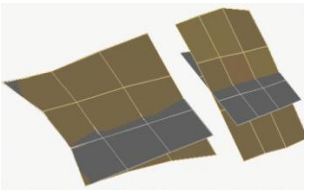
3	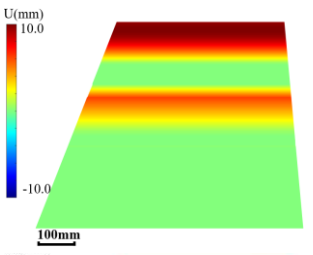	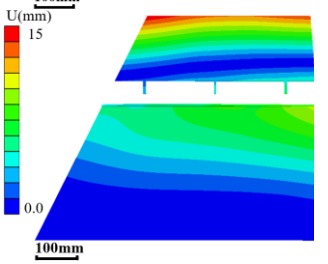	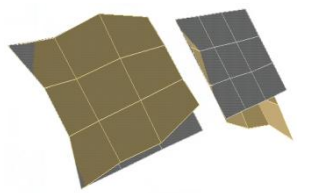
4	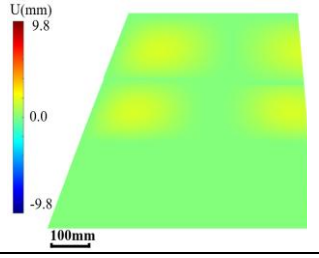	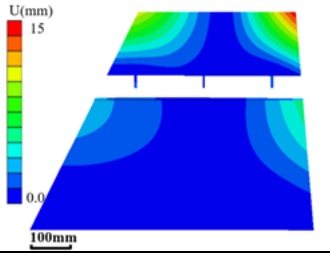	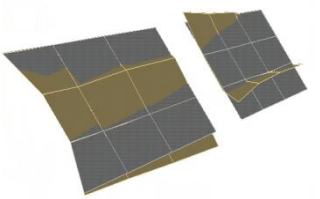

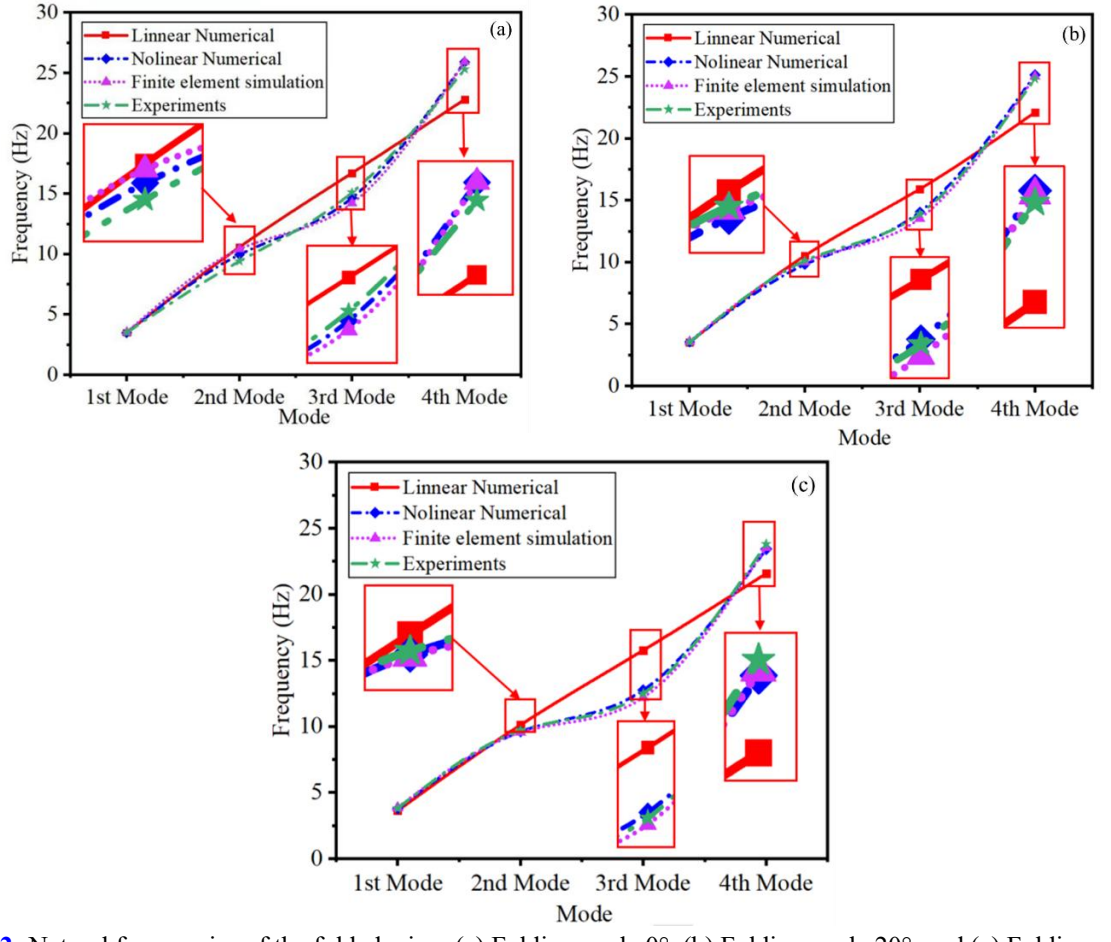

Fig. 12: Natural frequencies of the folded wing, (a) Folding angle 0°, (b) Folding angle 20°, and (c) Folding angle 40°.

Table 3: Frequency of vibration and error of the structure at 0° folding angle.

Model	1st	2nd	3th	4th
Experiment	3.5	9.4	15.1	25.3
Linear Numerical	3.49	10.57	16.71	22.8
Parameter Error	0.3%	12.4%	10.7%	9.9%
Nonlinear Numerical	3.49	9.94	14.64	26.01
Parameter Error	0.3%	5.7%	3%	2.8%

agreement with the results of the model experiment. The first two-order natural frequencies solved by the uncoupled linear dynamics equation have relatively high accuracy. However, there is a large error in solving the high-order natural frequencies, which does not conform to the real situation of the structure. Table 3 is the frequency of vibration and error of the structure at 0° folding angle, the data show that the vibration frequency errors of the rigid-flexible coupled nonlinear dynamics model for solving the structure are smaller than those of the linear model, which also confirms the high accuracy of the rigid-flexible coupled model. In conclusion, the data of the experimental model further verifies the accuracy of the rigid-flexible coupling dynamics equation.

6. Conclusion

This paper conducts an in-depth study on the nonlinear dynamic characteristics of the rigid-flexible coupling structure of the folding wing, and draws the following conclusions:

The proposed dynamic model of the rigid-flexible coupling structure is more consistent with the reality compared with the linear model. By simplifying the folding wing into a thin plate system, using the mixed coordinate method, Kirchhoff thin plate theory, assumed mode method and Lagrange equation, the nonlinear dynamic equations of the rigid-flexible coupling are successfully constructed, clearly revealing the coupling the influence of the additional stiffness caused by the flexible-rigid coupling deformation amount on the structure. The example analysis shows that the dynamic model with the additional stiffness of the rigid-flexible coupling deformation is more in line with the structural dynamic characteristics and motion laws. As the frequency of the driving torque increases, the vibration response of the dynamic system of the folding

wing increases. In the system without rigid-flexible coupling, the time-domain amplitude gradually increases until it diverges, while in the rigid-flexible coupling model, the vibration response increases slightly, and the overall trend remains unchanged.

The rigid-flexible coupling dynamic model has a high precision in solving the structural dynamic response. It is found in the study that the nonlinear deformation caused by the large deformation of the folding wing structure has little influence on the first two order natural frequencies. However, as the number of structural degrees of freedom increases, the calculation error gradually increases. There is no unified variation law for the natural frequencies under different Folding angles. The research taking the transverse external excitation as the control parameter shows that the calculation results of the nonlinear numerical model are highly consistent with those of the finite element method, which conforms to the characteristics of the vibration response. In the finite element model, there are slight differences between the linear and nonlinear calculation results.

The experimental model verifies the accuracy of the rigid-flexible coupling dynamic equations. An equivalent simplified model of the folding wing is manufactured based on the principles of functional and structural similarity and experiments are carried out. The vibration modes and natural frequencies under different Folding angles are obtained through the hammering method. The experimental results show that the first four order natural frequencies solved by the finite element model and the rigid-flexible coupling nonlinear dynamic equations are highly consistent with the experimental results, while there is a large error in solving the high order natural frequencies by the non-coupling linear dynamic equations. This further verifies the accuracy of the rigid-flexible coupling dynamic equations, providing a solid theoretical basis and technical support for the structural design and optimization of the folding wing, and it is of great significance for the development of the morphing aircraft.

In addition, the results of this study have certain feasibility for practical application in the design of folding wing aircraft, but also face some potential challenges. From a feasibility perspective, the rigid flexible coupled nonlinear dynamic equation constructed in this study can accurately describe the dynamic behavior of the folding wing in its working state, providing key theoretical references for the structural design of actual folding wing aircraft. In the process of structural design, key parameters such as stiffness and strength of the folding wing can be optimized based on this equation to achieve lightweight and high-performance folding wing aircraft.

However, applying the results of this research to the design of practical folding wing aircraft also faces some challenges. On the one hand, the actual flight environment is extremely complex, with multiple uncertain factors such as airflow disturbances, temperature changes, *etc.*, which can have a significant impact on the dynamic characteristics of folding wings. However, this study did not fully consider the comprehensive effects of these complex factors. On the other hand, in the actual manufacturing process, there may be a certain degree of discreteness in the material properties, and the manufacturing process may also introduce errors, which will lead to deviations between the dynamic characteristics of the actual structure and the theoretical model.

Conflict of Interest

There is no conflict of interest.

Acknowledgment

This work was supported by the National Natural Science Foundation of China (No. 51975085).

Supporting Information

Not applicable.

Reference

[1] S. Barbarino, O. Bilgen, R. M. Ajaj, M. I. Friswell, D. J. Inman, A review of morphing aircraft, *Journal of Intelligent Material Systems and Structures*, 2011, **22**, 823-877, doi: 10.1177/1045389x11414084.

[2] F. Afonso, J. Vale, F. Lau, A. Suleman, Performance based multidisciplinary design optimization of morphing aircraft, *Aerospace Science and Technology*, 2017, **67**, 1-12, doi: 10.1016/j.ast.2017.03.029.

[3] A. Karthik, D. S. Chiniwar, M. Das, P. Pai M, P. Prabhu, P. A. Mulimani, K. Samanth, N. Naik, Electric propulsion for fixed wing aircrafts - A review on classifications, designs, and challenges, *Engineered Science*, 2021, **16**, 129-145, doi: 10.30919/es8d573.

[4] D. Bye, P. McClure, Design of a Morphing Vehicle, *48th AIAA/ASME/ASCE/AHS/ASC Structures, Structural Dynamics, and Materials Conference*, Honolulu, Hawaii, AIAA, 2007, doi: 10.2514/6.2007-1728.

[5] R. M. Ajaj, M. S. Parancheerivilakkathil, M. Amoozgar, M. I. Friswell, W. J. Cantwell, Recent developments in the aeroelasticity of morphing aircraft, *Progress in Aerospace Sciences*, 2021, **120**, 100682, doi: 10.1016/j.paerosci.2020.100682.

[6] D. Grant, R. Lind, Effects of Time-Varying Inertias on Flight Dynamics of an Asymmetric Variable-Sweep Morphing Aircraft,

AIAA Atmospheric Flight Mechanics Conference and Exhibit, 20 August 2007 - 23 August 2007, Hilton Head, South Carolina. Reston, Virginia, AIAA, 2007, doi: 10.2514/6.2007-6487.

[7] H. Chen, B. Wang, X. Lin, K. A. Seffen, S. Zhong, Folding mechanics of a bistable composite tape-spring for flexible mechanical hinge, *International Journal of Mechanical Sciences*, 2024, **272**, 109188, doi: 10.1016/j.ijmecsci.2024.109188.

[8] J. Morley, Shape Optimization and modular discretization for the development of a morphing wingtip, University of Toronto, Ontario, Canada, 2012, ISBN: 978-0-494-91917-0.

[9] X. Guo, Y. Zhang, W. Zhang, L. Sun, S. Chen, Nonlinear dynamics of Z-shaped folding wings with 1: 1 inner resonance, *International Journal of Bifurcation and Chaos*, 2017, **27**, 1750124, doi: 10.1142/s0218127417501243.

[10] T. Lv, X. Zhang, J. Qiao, Y. Zhang, Y. Li, F. Yao, K. Yang, J. Shi, Theoretical research on dynamic modeling of rigid-flexible coupling system with double joint folded wing, *AIP Advances*, 2024, **14**, 045002, doi: 10.1063/5.0186002.

[11] M. Chang, Y. Sun, J.G. Bai, Aerodynamic design optimization of twice folding wing for tube-launched UAV constrained by flat-angle rotation mechanism, *Acta Aeronautica Astronautica Sinica*, 2022, **43**, 526331 -526331, doi: 10.7527/S1000-6893.2021.26331.

[12] J. Zhao, T. Cui, H. Zhao, Q. Qin, Characteristics of deploying longitudinal folding wings with compound actuation, *Advances in Mechanical Engineering*, 2024, **16**, 16878132241275598, doi: 10.1177/16878132241275598.

[13] D. H. Lee, P. C. Chen, Nonlinear aeroelastic studies on a folding wing configuration with free-play hinge nonlinearity, *47th AIAA/ASME/ASCE/AHS/ASC Structures, Structural Dynamics, and Materials Conference*, 1-4 May 2006, Newport, Rhode Island, Reston, Virginia: AIAA, 2006, doi: 10.2514/6.2006-1734.

[14] Y. Huang, X. Guo, D. Cao, Aerodynamic characteristics of a Z-shaped folding wing, *Aerospace*, 2023, **10**, 749, doi: 10.3390/aerospace10090749.

[15] W. Hu, Z. Yang, Y. Gu, Aeroelastic study for folding wing during the morphing process, *Journal of Sound and Vibration*, 2016, **365**, 216-229, doi: 10.1016/j.jsv.2015.11.043.

[16] Y. Fu, A. Xiao, B. Liu, Boundary control for an unmanned aerial vehicle with a nonhomogeneous rigid-flexible coupling wing, *Chinese Journal of Engineering*, 2024, **9**, 1574-1581, doi: 10.13374/j.issn2095-9389.2023.09.30.001.

[17] R. Huang, X. Zhou, Parameterized fictitious mode of morphing wing with bilinear hinge stiffness, *AIAA Journal*, 2021, **59**, 2641-2656, doi: 10.2514/1.J059347.

[18] R. Yang, X. Lu, X. Huang, W. Qian, S. Sun, Dynamic characterization of folded wing flutter model based on substructure mode synthesis method, *International Journal of Structural Stability and Dynamics*, 2025, **3**, 2650136, doi: 10.1142/s0219455426501361.

[19] J. Chen, W. Hu, Q. Li, Nonlinear dynamics of a foldable multibeam structure with one to two internal resonances, *International Journal of Mechanical Sciences*, 2019, **150**, 369-378, doi: 10.1016/j.ijmecsci.2018.10.034.

[20] K. Huang, J. Zhang, Q. Wang, Natural vibration analysis of two-dimensional flexible wing based on non-uniform beam model, *Chinese Journal of Theoretical and Applied Mechanics*, 2023, **2**, 487-497, doi: 10.6052/0459-1879-22-551.

[21] W. Su, CES. Cesnik, Strain-based geometrically nonlinear beam formulation for modeling very flexible aircraft, *International Journal of Solids and Structures*, 2011, **48**, 16-17, doi: 10.1016/j.ijsolstr.2011.04.012.

[22] X. Guo, S. Wang, Y. Qu, D. Cao, Nonlinear dynamics of Z-shaped morphing wings in subsonic flow, *Aerospace Science and Technology*, 2021, **119**, 107145, doi: 10.1016/j.ast.2021.107145.

[23] M. L. Verstraete, B. A. Roccia, D. T. Mook, S. Preidikman, A co-simulation methodology to simulate the nonlinear aeroelastic behavior of a folding-wing concept in different flight configurations, *Nonlinear Dynamics*, 2019, **98**, 907-927, doi: 10.1007/s11071-019-05234-9.

[24] K. Tian, Y. Wang, D. Cao, K. Yu, Approximate global mode method for flutter analysis of folding wings, *International Journal of Mechanical Sciences*, 2024, **265**, 108902, doi: 10.1016/j.ijmecsci.2023.108902.

[25] W. Qi, Y. Li, Z. Zhang, S. Tian, Aerodynamic characteristics of unmanned aerial vehicle with Z-shaped folding wings, *Journal of Aircraft*, 2025, **11**, 1-15, doi: 10.2514/1.C038324.

[26] S. Yan, Y. Zhou, S. Jiang, H. Xue, P. Guo, Design and aerodynamic analysis of a flapping mechanism for foldable biomimetic aircraft, *Biomimetics*, 2025, **10**, 61, doi: 10.3390/biomimetics10010061.

[27] W. Pu, Q. Shen, Y. Lu, Y. Yan, Y. Yang, Structure design and kinematic modeling of a robotic bird attitude transformation mechanism based on avian flight characteristics, *Biomimetics*, 2025, **10**, 131, doi: 10.3390/biomimetics10030131.

[28] Z. Li, G. Jin, T. Ye, T. Yang, Y. Chen, Dynamic analytical modeling and vibration characteristics analysis of periodic corrugated sandwich structures, *Journal of Vibration Engineering*, 2025, **1**, 19-28 doi: 10.16385/j.cnki.issn.1004-4523.2025.01.003.